Economic Geology, v. 84, pp. 229-255
https://doi.org/10.2113/gsecongeo.84.2.229

ECONOMIC GEOLOGY

AND THE

BULLETIN OF THE SOCIETY OF ECONOMIC GEOLOGISTS

VOL. 84 MARCH–APRIL, 1989 NO. 2

Paleohydrologic Evolution and Geochemical Dynamics of Cumulative Supergene Metal Enrichment at La Escondida, Atacama Desert, Northern Chile

CHARLES N. ALPERS* AND GEORGE H BRIMHALL

Department of Geology and Geophysics, University of California, Berkeley, California 94720

Abstract

Quantitative limonite mapping within the leached capping of the porphyry copper deposit at La Escondida, Chile, permits reconstruction of the paleohydrologic and chemical evolution of a well-developed supergene ore-forming system. The mineralogy, textures, and relative abundance of supergene limonite minerals (hematite, goethite, and jarosite) are used to reconstruct the former ratio of pyrite to chalcocite and the preoxidation copper grade based on empirical limonite sulfide correlations (after Locke, 1926; Blanchard, 1968; and Loghry, 1972). Estimates of preoxidation copper grades in surface exposures and tops of drill holes at La Escondida are significantly lower than actual copper grades in the underlying enrichment blanket at depth. This apparent inconsistency is explained by a progressive increase in the copper grade of the sulfide enrichment blanket as it descended to its present location in response to a descending water table. This systematic trend of reconstructed grades of supergene-enriched copper sulfide increasing with depth offers the first quantitative proof of cumulative downward enrichment in a supergene profile, as proposed by Locke (1926). The consistent trends of limonite mineralogy and abundance in vertical profiles indicate that water table descent at La Escondida was relatively continuous in space, although not necessarily in time.

Evidence for cumulative downward enrichment in vertical profiles through leached capping allows quantitative analysis of chemical mass balance in dynamic supergene systems. Slopes of linear regressions for profiles of reconstructed enriched copper grades vs. depth indicate lateral fluxes into or out of a given vertical profile. This method provides independent verification of conclusions from a previous study of copper mass balance at La Escondida (Brimhall et al., 1985) which showed that lateral fluxes of copper were a significant factor during supergene leaching and enrichment.

Introduction

THE principal objective of the present study is to understand the dynamic chemical and hydrologic evolution of supergene leaching and enrichment processes through detailed study of a well-enriched copper sulfide deposit. In general, the understanding of dynamic aspects of geochemical processes has been advanced by the study of systems in which intermediate states of evolution have been preserved. Two examples are multistage hydrothermal vein deposits where paragenetic sequences may be deduced from textural and fluid inclusion evidence (e.g., Kelly and Turneaure, 1970; Kamilli and Ohmoto, 1977; Loucks, 1982) and metamorphic rocks for which pressure-temperature-time paths can be established by combined geochronologic, petrologic, and petrographic studies (e.g., England and Thompson, 1984). Preserved intermediate states provide the most rigorous constraint on dynamic models for geochemical and hydrologic processes which commonly operate over time scales inaccessible by direct field observation or by laboratory simulation. In this study, we describe the oxidative weathering of sulfide-bearing rocks as an example of a hydrochemical transport process for which intermediate states of a dynamic geochemical system may be deduced from quantitative analysis of the rock record.

We focus on the porphyry copper deposit at La Escondida, Chile, a deposit as yet unmined, where

* Present address: U. S. Geological Survey, Mail Stop 420, 345 Middlefield Road, Menlo Park, California 94025.

0361-0128/89/908/229-27

the effects of supergene processes are extremely well developed (Brimhall et al., 1985; Alpers, 1986). The present hyper-arid climate of the Atacama Desert has preserved supergene-enriched sulfide ore deposits in this region (Sillitoe et al., 1968; Mortimer, 1973; Mortimer et al., 1977; Sillitoe, 1981) through a marked decrease in the long-term average rate of erosion since the middle Miocene (Mortimer and Sarič-Rendic, 1975; Alpers et al., 1984; Alpers and Brimhall, 1988). Climatic desiccation may have also played an important role in the formation of supergene-enriched sulfide deposits in this region by contributing to water table descent which would have provided optimal conditions for cumulative supergene enrichment effects (Locke, 1926; Bateman, 1950; Alpers and Brimhall, 1988).

In this paper, we describe the mineralogic and hydrologic factors which controlled the progress and extent of supergene copper leaching and enrichment at La Escondida and the formation of residual limonite minerals in the leached capping zone. Our approach combines classical methods of leached capping appraisal (Locke, 1926; Blanchard, 1968; Loghry, 1972) with more recently developed methods of mass balance analysis which are the basis for reconstruction of paleotopography, paleohydrology, and estimation of long-term average rates of erosion and uplift (Brimhall et al., 1985; Alpers, 1986; Brimhall and Dietrich, 1987; Alpers and Brimhall, 1988).

Under conditions of a descending ground-water table, the relative rates of sulfide oxidation and groundwater table descent determine the overall efficiency of supergene leaching and enrichment processes. We use the results of quantitative limonite mapping at La Escondida to constrain these relative rates by comparison of algebraic models for the geochemical dynamics of an evolving supergene system.

Methods of Leached Capping Interpretation

Previous work

Quantitative interpretation of leached cappings over copper ores was first described by Locke (1926) and Tunell (1930). An essential feature of this early work was the observation that deep maroon to seal brown, hematitic iron oxide tends to remain in rocks after oxidation of supergene chalcocite-bearing ores which form as the enrichment product of chemical weathering of copper-iron sulfide protores. The sulfide mineralogy of supergene chalcocite ores is complex in detail, probably consisting of a fine-grained mixture including some or all of the following: low chalcocite ($Cu_{1.995-2.000}S$), djurleite ($Cu_{1.934-1.965}S$), digenite ($Cu_{1.70-1.74}Fe_{0.05-0.01}S$), and anilite ($Cu_{1.75}S$) (Sillitoe and Clark, 1969; Clark and Sillitoe, 1971; Morimoto and Gyobu, 1971; Potter, 1977). Vertical zoning of these minerals and the occurrence of covellite in supergene profiles is discussed in a later section of this paper. For the purposes of the following discussion, we approximate the sulfide mineralogy in the upper portions of copper sulfide enrichment blankets as consisting solely of supergene chalcocite and residual hypogene pyrite, where "chalcocite" refers to all copper-iron sulfides with a Cu/S molar ratio greater than 1.70 and an Fe/S ratio less than 0.05. As discussed below, pyrite plus chalcocite is a reasonable approximation for the uppermost 100 to 300 m of the enrichment blanket at La Escondida.

Numerous field and laboratory investigations of leached cappings over porphyry copper deposits have led to successful empirical correlations of the mineralogy, texture, and abundance of leached capping limonite minerals (hematite, goethite, and jarosite) with underlying sulfide assemblages. These correlations depend on the nature and extent of local iron fixation (Blanchard, 1968; Loghry, 1972). Quantitative limonite mapping over chalcocite-pyrite ores permits reconstruction of sulfide assemblages prior to leaching in terms of the total former sulfide volume, V_α, former pyrite to chalcocite ratio, $(py/cc)_\alpha$, and former total copper grade prior to oxidation, b_α. The variable b_α was introduced (as b^α) by Brimhall et al. (1985) to signify the average metal grade of an enrichment blanket zone at the earlier stage of a two-stage enrichment process. In this paper, we broaden this definition to consider b_α as the average blanket grade at any former stage of supergene evolution.

Stages of supergene enrichment blanket evolution have been resolved at several individual deposits based on the interpretation of limonite variations with elevation within the leached capping zones. For example, Richard and Courtright (1958), Tosdal (1978), and Anderson (1982) have concluded that a relatively sudden drop in the water table resulted in the observed vertical limonite profile of hematitic above jarositic capping at Toquepala, Peru. Multiple stages of leaching and enrichment have also been described at several porphyry copper deposits in Arizona, including Morenci-Metcalf (Langton, 1972) and Sacaton (Cummings, 1982). Similar principles were used by Gaskin (1975) to deduce three stages of supergene development in lateritic iron ores from banded ironstones at Tonkalili, Sierra Leone, based on the distribution of limonite-enriched and limonite-deficient zones in vertical weathering profiles. In the above examples, observed discontinuities in limonite distribution were used to infer discrete stages or cycles of supergene evolution. In contrast, the observation of relatively continuous variations in the mineralogy and abundance of iron oxides in vertical profiles can be used to infer a relatively continuous descent of the water table during supergene enrichment such as at San Xavier North, Arizona (King, 1982), Chino, New Mexico (Anderson, 1982), and La Escondida, Chile (Alpers, 1986; this study).

The distinction between indigenous and trans-

ported limonite is of critical importance to the interpretation of leached outcrops. As defined by Blanchard (1968, p. 11), "Indigenous limonite is that precipitated from iron-bearing solutions within the cavity or space formerly occupied by the sulfide or other mineral from which the iron is derived." In this study, we consider "indigenous limonite" to be the limonite occupying former sulfide sites; it is unnecessary for our purposes to assume that the iron in these sites was locally derived so long as it represents a replacement of sulfide. In contrast to indigenous limonite, we consider transported limonites ("exotic limonites" of Blanchard, 1968) to represent iron which has clearly moved from its original source and has precipitated in nonsulfide sites, generally in fractures or as a pervasive stain. Limonite precipitated on the borders of the former sulfide sites, previously described as fringing (Blanchard, 1968) or contiguous (Locke, 1926), is considered here as a subset of transported limonites (cf. Loghry, 1972).

The distinction between indigenous and transported limonites is straightforward for oxidation products of disseminated sulfide grains. Limonite in veins and fractures may be transported or may represent indigenous limonite replacing sulfide veins; this ambiguity is resolvable by the observation of siliceous sponge limonite, indicative of previous massive sulfide mineralization (Blanchard, 1968; Andrew, 1980). Although some of the iron in sponge limonite may not be locally derived, boxwork textures and sponge limonite are considered to represent former sulfide sites, and thus, are included as a form of indigenous limonite in this study. As discussed below, the volume of voids associated with indigenous limonite is used to estimate the volume percent of sulfides prior to oxidation, V_α, which is an important parameter for reconstructing preleaching metal grades.

A wide variety of limonite textures has been described in gossans and leached cappings (Blanchard, 1968; Loghry, 1972; Blain and Andrew, 1977; Andrew, 1980). For chalcocite-pyrite ores, the texture and mineralogy of indigenous limonites vary systematically with the original pyrite/chalcocite ratio (Table 1). In relatively nonreactive gangue, including phyllic and advanced argillic alteration, the oxidation of sulfide mixtures with $(py/cc)_\alpha$ less than about 1.5:1 is observed to form only hematite. According to the limonite-sulfide correlations by Loghry (1972), a minimum $(py/cc)_\alpha$ ratio of 1:2.8 is necessary to ensure that pH stays low enough so that cupric hydroxy-sulfates such as antlerite and brochantite do not form and so that the maximum possible amount of copper is mobilized. According to Loghry's correlations, with increasing $(py/cc)_\alpha$ ratio, a systematic increase in the

TABLE 1. Textures and Relative Abundances of Limonites Formed from Various Initial Ratios of Pyrite/Chalcocite (after Loghry, 1972)

Slow neutralizers Phyllic, argillic, or advanced argillic alteration			Relative abundance			Moderate neutralizers Potassic, propylitic, or weak phyllic alteration	
X_{Cu}[2]	$(py/cc)_\alpha$	Indigenous limonites[1]	Indigenous	Transported	Transported limonites[1]	$(py/cc)_\alpha$	X_{Cu}[2]
—[3]	1:2.8+	None	—	—	None	1:2.5+	—[3]
1.23	1:2.5	H; fragile, *relief*, fine cellular	10	0	H; none or rare	1:2.0	1.16
1.16	1:2					1:1.5	1.06
1.06	1:1.5		9	1		1:1	0.92
0.92	1:1	H; *relief*, hard cellular	8	2	H; *fringing*	1.5:1	0.75
0.75	1.5:1	H; *relief*, hard cellular, *rare botryoidal*	7	3	H; fringing, exotic (in fractures)	2:1	0.64
0.64	2:1	H ⩾ G; *botryoidal*, hard cellular, relief	6	4		3:1	0.49
0.49	3:1	H > G; botryoidal, hard compact, rare relief	5	5	H > G (>J); fringing, exotic, rarely iridescent	4:1	0.40
0.40	4:1	H ≅ G; *nodular*, hard compact, vitreous, flat	4	6	G > H (≅J); iridescent	5:1	0.33
0.33	5:1	G > H	3	7	J ≅ G > H		
0.25	7:1	(G + J) > H	2	8	J > G > H		
0.20	10:1	G + J	1	9	J > G		
<0.10	>20:1	None	0	10	J		

[1] G = goethite, H = hematite, J = jarosite; italics indicate diagnostic hematite textures

[2] X_{Cu} = multiplication factor equal to percent copper per volume percent indigenous limonite (V_α); based on copper content and specific gravity of sulfides (from Loghry, 1972)

[3] Insufficient acid for complete leaching; produces abundant copper oxides and hydroxy-sulfates

proportion of indigenous goethite relative to hematite is observed, along with systematic changes in the morphology of the limonites (Table 1, Fig. 1).

Variations in the relative proportion of indigenous vs. transported limonites with increasing $(py/cc)_\alpha$ ratio have long been known qualitatively (Locke, 1926; Blanchard, 1968; Loghry, 1972; Andrew, 1980). The two central columns of Table 1 were added by Alpers (1986) to table 7 of Loghry (1972), taking into account semiquantitative observations described by Smith (unpub. data, 1950) reproduced by Loghry (1972), Blanchard (1968), and Loghry (1972) regarding the systematic increase of transported limonite with increasing $(py/cc)_\alpha$ ratio. The inverse relationship of transported vs. indigenous limonite is shown graphically in Figure 1. Transported (mostly fringing) limonites are observed for $(py/cc)_\alpha$ ratios greater than about 1:2; they increase in abundance relative to indigenous limonite with increasing $(py/cc)_\alpha$. As with the indigenous limonites, transported limonites show a systematic change in mineralogy from hematite to goethite to jarosite with increasing $(py/cc)_\alpha$ ratios. With $(py/cc)_\alpha$ ratios greater than 10:1, nearly all limonite is transported and commonly occurs as jarosite with minor goethite.

Figure 1 and the left side of Table 1 pertain to rocks with little or no capacity to neutralize supergene acids, such as advanced argillic and phyllic alteration assemblages. The right side of Table 1 shows the $(py/cc)_\alpha$ ratios and associated limonite textures and mineralogy for rocks of moderate acid-neutralizing capacity, including potassic and propylitic alteration assemblages. The more reactive gangue minerals such as feldspars, chlorite, and biotite inhibit the transport of iron by consumption of hydrogen ions through hydrolysis reactions, so that a given characteristic limonite texture and mineral assemblage corresponds to a higher $(py/cc)_\alpha$ ratio for more reactive gangue. Rocks of strong acid-neutralizing capacity such as carbonates require yet a different scale; however, rocks of this type were not encountered in this study.

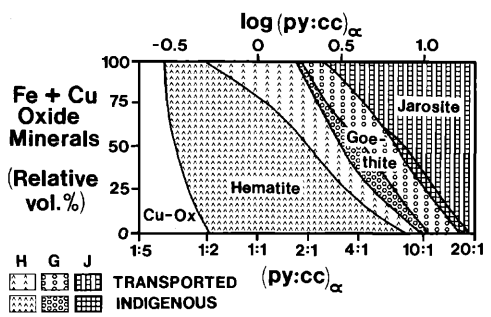

FIG. 1. Graphical representation of logarithmic scale correlations between limonite mineralogy and original pyrite/chalcocite ratios in rocks prior to oxidation, for nonreactive gangue (argillic, advanced argillic, and phyllic alteration). Based largely on Smith (1950) and Loghry (1972), who synthesized observations from several porphyry copper deposits in southwestern North America (see Table 1 and text). See text for discussion of distinction between indigenous limonites (continuous patterns on figure) and transported limonites (vertically striped patterns).

Theoretical and experimental basis for pH control of limonite-sulfide correlations

Empirical correlations between the relative abundance of sulfide reactants and the mineralogy, texture, and abundance of limonite products can be understood by consideration of reaction stoichiometry together with data on the solubility and formation kinetics of various secondary iron minerals as a function of pH. The composition of oxidizing sulfides, in particular, the molar metal to sulfur ratio (Me/S), apparently has an important influence on the pH of the resulting supergene solutions (Blanchard, 1968; Thornber, 1975; Blain and Andrew, 1977; Andrew, 1980). In detail, the effective surface areas (Aagaard and Helgeson, 1982) of sulfide grains undergoing reaction at a given time will determine the effective Me/S ratio; so, in the case that there are significant variations in sulfide grain size and shape, the effective Me/S ratio will not correspond necessarily to the bulk-ore composition.

The actual mechanisms and rates of sulfide oxidation reactions in nature are complex and in need of further study (Nordstrom, 1982; Goldhaber, 1983). Nevertheless, simplified examples of overall sulfide dissolution reactions using $O_{2(aq)}$ as the oxidant (Table 2) illustrate the potential importance of the Me/S ratio in determining solution pH. In general, the oxidative dissolution of pyrite is the dominant source of sulfuric acid in the weathering of sulfide deposits (Nordstrom, 1982), not only because pyrite is the most common sulfide in the upper crust but also because of its stoichiometry (Me/S = 1:2). Note that formation of solid products other than $Fe(OH)_3$, such as goethite or hematite, from oxidative pyrite dissolution would also produce four moles of H^+ per mole of pyrite, consuming less water than the reaction shown in Table 2. Many other common sulfides (e.g., ZnS, PbS, CuS, and $CuFeS_2$) have Me/S = 1:1; oxidative dissolution of these minerals has relatively less effect on solution pH if the oxidant is $O_{2(aq)}$. In contrast, the copper sulfides in supergene chalcocite (djurleite, digenite, anilite, etc.) have Me/S ratios closer to 2:1, which causes the oxidative dissolution reactions, as written in Table 2, to consume hydrogen ions. Oxidation of metal sulfides by aqueous Fe^{+3} (Dutrizac and MacDonald, 1974; Nordstrom, 1982) may temporarily produce eight moles of H^+ in solution per mole of sulfide; however, the acid is subsequently consumed when the product aqueous Fe^{+2} is reoxidized (Singer and Stumm, 1970; Davison and Seed, 1983). The formation of aqueous complexes containing H and OH will also have an important effect on determining the pH of the oxidizing solution, but this effect

TABLE 2. Sulfide Oxidation Reactions

Metal/Sulfur ratio		
1:2	Pyrite $FeS_2 + 3.75O_2 + 3.5H_2O$	$\rightarrow Fe(OH)_3 + 2SO_4^{-2} + \underline{\underline{4H^+}}$
1:1	Covellite $CuS + 2O_2$	$\rightarrow Cu^{+2} + SO_4^{-2}$
1.75:1	Anilite (Digenite) $Cu_{1.75}S + 2.375O_2 + \underline{\underline{1.5H^+}}$	$\rightarrow 1.75Cu^{+2} + SO_4^{-2} + 0.75H_2O$
2:1	Chalcocite $Cu_2S + 2.5O_2 + \underline{\underline{2H^+}}$	$\rightarrow 2Cu^{+2} + SO_4^{-2} + H_2O$

__ has been added for emphasis

is secondary to the stoichiometry of the reactant sulfides.

Hematite vs. goethite formation: Numerous studies have attempted to resolve the environmental factors which determine the formation of hematite vs. goethite during chemical weathering, yet this subject remains enigmatic. The thermodynamic stability relations between hematite and goethite are governed by the simple hydration reaction:

$$Fe_2O_3 + H_2O = 2FeO(OH). \quad (1)$$

However, the actual mechanism of transformation between these phases is considerably more complicated, as discussed below. Although hematite and goethite are often found together as weathering products in nature, the phase rule dictates that only one of these two phases is stable thermodynamically in the Fe_2O_3-H_2O system at a given pressure, temperature, and activity of water, except on the univariant phase boundary. Attempts to explain the relative abundance of hematite and goethite in various geologic settings based on thermodynamic properties (Posnjak and Merwin, 1922; Berner, 1969, 1971; Langmuir, 1971, 1972; Langmuir and Whittemore, 1971; Whittemore, 1973; Bladh, 1978, 1982; Murray, 1979) have shown that the two phases are very close in solubility and therefore in thermodynamic stability. The thermodynamic properties of ferric oxide and oxyhydroxide minerals may be influenced to an important degree by aluminum substitution, which can range up to 33 mole percent AlO(OH) in goethite, and up to 14 mole percent Al_2O_3 in hematite (Yapp, 1983; Tardy and Nahon, 1985; Schwertmann, 1985; Trolard and Tardy, 1987). Grain size effects (Langmuir, 1971, 1972; Murray, 1979) are also important with respect to the thermodynamic stability relations; however, consideration of these effects does not explain all field occurrences in soils (Schwertmann, 1985).

If pH is the most important controlling factor, the relationships in Figure 1 and Tables 1 and 2 suggest that goethite would be favored at a pH intermediate between that favorable to jarosite and hematite. The available results from experimental and field studies support this suggestion for both kinetic and thermodynamic reasons, yet relatively few studies (Schwertmann, 1965, 1969; Whittemore, 1973; Knight and Sylva, 1974; Schwertmann and Murad, 1983) have addressed the issue of pH control on limonite mineralogy. According to Schwertmann (1985), the important factors influencing hematite vs. goethite formation and transformation in soils include temperature, water activity (expressed as either humidity or degree of saturation), pH, organic matter, and release rate of Fe during weathering. In addition, the abundances of aqueous ferrous iron and sulfate may be important factors in determining the mineralogy of ferric iron precipitates (Feitknecht and Michaelis, 1962; Whittemore, 1973; Brady et al., 1986).

Ferrihydrite is a poorly crystalline mineral found in soils (Chukhrov et al., 1973; Schwertmann, 1985), formerly considered to be amorphous $Fe(OH)_3$ by many workers. The stoichiometry of ferrihydrite remains controversial; Russell (1979) proposed the structural formula $Fe_2O_3 \cdot 2FeO(OH) \cdot 2.6H_2O$, corresponding to $Fe_2O_3 \cdot 1.8H_2O$, based on Mössbauer spectroscopy, whereas Eggleton and Fitzpatrick (1988) suggest that ferrihydrite composition is best described as between $Fe_4(O,OH,H_2O)_{12}$ and $Fe_{4.6}(O,OH,H_2O)_{12}$, depending on crystal size. Ferrihydrite has been shown to be the necessary precursor to supergene hematite, to which it transforms by solid state dehydration (Feitknecht and Michaelis, 1962; Schwertmann, 1965, 1985; Schwertmann and Fischer, 1965; Chukhrov et al., 1973). When this transformation takes place in water, there is a competing tendency for ferrihydrite to dissolve back into solution and for the ferric iron to reprecipitate as fine-grained goethite. Under weathering conditions, goethite and hematite are not related genetically by the simple hydration-dehydration reaction in eq. (1); rather, the two phases form by separate pathways (Fischer and Schwertmann, 1975; Schwertmann, 1985).

The possibility that the competitive nature of these reaction mechanisms could lead to different results

under different conditions led Schwertmann and Murad (1983) to conduct a series of long-term experiments in which ferrihydrite was aged at a wide range of pH for up to several years (Fig. 2). Both hematite and goethite were produced at each pH and maximum hematite production occurred at pH = 8. Goethite was the dominant phase produced below pH = 6 and above pH = 9. The relevance of these experimental results to natural systems is supported by the study of 11 soils from southern Brazil (Kämpf and Schwertmann, 1982), which showed an increasing proportion of hematite with increasing pH in the range of 4 to 6.

Other dissolved ions may also play an important role in determining goethite vs. hematite formation. For example, Ca^{+2} and Mg^{+2} have been found to favor hematite over goethite (Schellmann, 1959; Taylor and Grayley, 1967; Torrent and Guzman, 1982) and dissolved sulfate can suppress goethite formation completely under certain conditions (Torrent and Guzman, 1982; Brady et al., 1986). Also important to the subject of chalcocite-pyrite oxidation is the observation that Cu^{+2} can catalyze the oxidation of Fe^{+2} to Fe^{+3} by $O_{2(aq)}$ (Thornber, 1985), leading to formation of ferrihydritelike precipitates which may convert to hematite if aged under favorable conditions. Thornber (1985) asserted that indigenous limonite textures showing preexisting crystal forms would indicate a pH greater than 6. Thus, the observation that indigenous, hematitic limonites commonly replace sulfide assemblages relatively high in chalcocite (Table 1, Fig. 1) may be in part explained by the catalytic oxidation of Fe^{+2} by Cu^{+2} at relatively high pH.

Within a single weathered sulfide deposit, the hematitic and goethitic zones share a similar environmental history, including temperature and degree of hydrodynamic saturation (water activity). The other important factors besides pH which are discussed by Schwertmann (1985) as influencing hematite vs. goethite formation (organic matter, release rate of Fe, and presence of Fe^{+2} and other dissolved ions) are themselves to some degree dependent on pH. The role of organic matter is to suppress hematite formation by complexation of Fe(III) in solution, which may prevent the formation of ferrihydrite (Schwertmann, 1985). The effects of organic matter and bacteria are largely inseparable from other environmental factors such as climate and vegetation when comparing different deposits and soil profiles. However, the differential effects of organic matter between goethitic and hematitic zones at a single deposit could depend on the pH of the pore fluids, which in turn depends on soil chemistry, wall-rock alteration, and original sulfide mineralogy. The release rate of Fe during weathering will also depend on pH and biological activity, given available data for kinetics of pyrite and aqueous Fe^{+2} oxidation (Whittemore, 1973; Nordstrom, 1982, and references therein; Davison and Seed, 1983; Wiersma and Rimstidt, 1984).

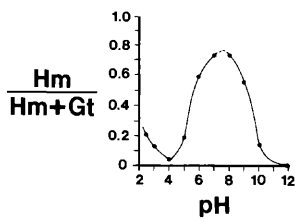

FIG. 2. Results of Schwertmann and Murad (1983) for experimental aging of ferrihydrite at a range of pH conditions: hematite/(hematite + goethite) (Hm/(Hm + Gt)) ratios vs. pH after 441 days of storage at 25°C. Reproduced by permission of the Clay Minerals Society and the authors.

Jarosite formation: Jarosite (ideally $KFe_3(SO_4)_2(OH)_6$) is known to precipitate at low pH conditions in natural and perturbed systems associated with pyrite oxidation, such as acid sulfate soils and acid mine drainages (van Breemen, 1973; Nordstrom et al., 1979; Nordstrom, 1982; Chapman et al., 1983). Although there are large uncertainties associated with the available thermodynamic data (Nordstrom, 1977; Chapman et al., 1983; Nordstrom and Munoz, 1986; Alpers et al., 1988), the thermodynamic stability of jarosite relative to goethite and ferrihydrite is displayed on pE-pH diagrams in Figure 3A and B (thermodynamic data are listed in Appendix I). The relatively concentrated solutions depicted in Figure 3A are similar to extremely acid mine waters (pH as low as 0.80) from Iron Mountain, West Shasta district, California, which are known to form jarosite upon oxidation (Nordstrom, 1977; Alpers et al., 1988, 1989). In the more dilute conditions depicted in Figure 3B, jarosite does not have a field of thermodynamic stability relative to goethite (pK = 41.7) or hematite (pK = 41.6) but is stable relative to ferrihydrite (pK = 39). The relations in Figure 3B may pertain to conditions in soils, where ferrihydrite or other poorly crystalline precipitates are the initial products of iron hydrolysis.

Appreciable solid solution between potassium, sodium, and hydronium end members is found in natural and synthetic jarosites (Kubisz, 1964, 1970; Brophy and Sheridan, 1965; Dutrizac, 1983; Alpers et al., 1988, 1989). Problems with iron deficiency and excess water have been reported in both jarosites and alunites (Kubisz, 1970; Dutrizac and Kaiman, 1976; Härtig et al., 1984; Ripmeester et al., 1986; Bohmhammel et al., 1987); however, these substitutions do not affect the conclusion that jarosites form at lower pH than ferric oxides and oxyhydroxides (Brown, 1971; van Breemen, 1973; Bladh, 1978; Dutrizac, 1982). The thermodynamic stability of jarosite at lower pH than ferrihydrite is in accord with the

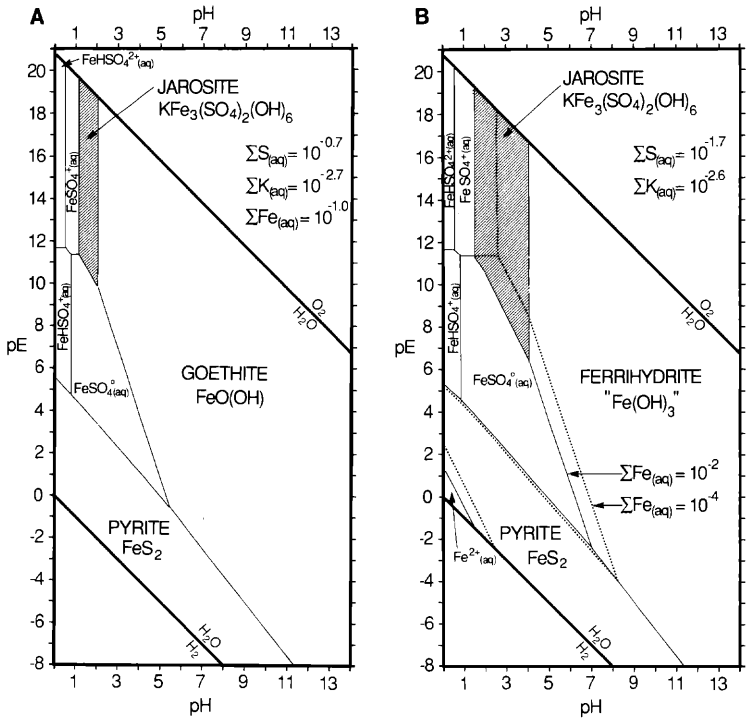

FIG. 3. A. pE-pH diagram for the Fe-S-K-O-H system at 25°C, 1 bar, with total aqueous sulfur activity of $10^{-0.7}$, total aqueous potassium activity of $10^{-2.7}$, and total aqueous iron activity at 10^{-1}. Thermodynamic data and sources are listed in Appendix I. Jarosite field is ruled. Crystalline sulfur and iron sulfides other than pyrite are not included. B. pE-pH diagram for the Fe-S-K-O-H system at 25°C, 1 bar, with total aqueous sulfur activity of $10^{-1.7}$, total aqueous potassium activity of $10^{-2.6}$, and total aqueous iron activity of 10^{-2} (solid lines) and 10^{-4} (dotted lines). Thermodynamic data and sources are listed in Appendix I. Jarosite field is ruled. Goethite, hematite, crystalline sulfur, and iron sulfides other than pyrite are not included.

observations that jarosite-rich limonite assemblages are associated with oxidation of sulfide assemblages with high relative pyrite contents and low Me/S ratios (Table 1, Fig. 1).

Methods used in this study

The methods of quantitative leached capping interpretation used in this study are an extension of the methods described by Loghry (1972). It is assumed that the volume of voids associated with indigenous limonite represents the former volume of sulfides prior to oxidation and copper leaching, V_α. The empirically calibrated scales in Table 1 and Figure 1 were used to estimate the former ratio of pyrite to chalcocite, $(py/cc)_\alpha$. For each value of $(py/cc)_\alpha$ and the appropriate scale of gangue reactivity, a multiplication factor (X_{Cu}, Table 1) based on mineral stoichiometry and specific gravity was used to convert V_α to an estimate of total weight percent copper leached. Any residual copper in the rock, of grade l_R, was then added to the estimate of total copper leached to determine the estimated total copper grade prior to leaching, b_α. Thus, the overall formula is $b_\alpha = V_\alpha \cdot X_{Cu} + l_R$. The rationale for the addition of residual copper is that the grade reconstruction pertains to copper leached from the rock and presumably transported out of the rock volume which represents the mapping interval (Loghry, 1972) (see Table 3 for complete list of symbols).

Surface limonite mapping at La Escondida was accomplished by systematic sampling of available surface bedrock exposures, most of which consisted of manmade roadcuts and trenches of 1 to 5 m depth. Surface float samples, used in the initial evaluation of the property (J. D. Lowell and J. H. Courtright, pers. commun., 1982), were found to be much less representative than bedrock samples due to weathering out of key limonite textures. Each 5 m, where possible, a bedrock sample of at least 500 g was taken, representative of limonite texture, mineralogy, and abundance. Field notes concerning limonite textures, mineralogy, and abundance were supplemented by careful examination with a binocular microscope (10×–60×). Quantitative mineralogic data were composited mentally for groups of up to 20 samples, each group representing as much as 100 m of outcrop. Smaller composites were made where macroscopic

TABLE 3. List of Symbols

Symbol	Description	Units
b	Average metal grade within enrichment blanket	Weight percent metal
b_α	Reconstructed average copper grade of enriched zone prior to oxidation; based on limonite interpretation	Weight percent metal
b_{max}	Maximum average metal grade within enriched blanket	Weight percent metal
B	Enrichment blanket thickness	Meters
EBB	Elevation of bottom of enrichment blanket	Meters (elevation)
ETB	Elevation of top of enrichment blanket	Meters (elevation)
flux	Lateral transfer of metal into (+) or out of (−) control volume	Grams per cm^2
l	Average metal grade within leached capping	Weight percent metal
l_{min}	Minimum average metal grade within leached capping	Weight percent metal
l_R	Residual copper grade in leached capping interval used in grade reconstruction	Weight percent metal
L_T	Open-system total leached column height	Meters
L_T^0	Calculated total leached column height assuming a closed system, i.e., zero lateral flux	Meters
$L_{T,\alpha}$	Total leached column height based on reconstructed blanket grades prior to oxidation of leached capping	Meters
p	Average metal grade within protore	Weight percent metal
(py/cc)	Volume ratio of pyrite to chalcocite	Unitless number
$(py/cc)_\alpha$	Reconstructed (py/cc) prior to oxidation for rocks previously enriched, now leached; based on limonite interpretation	Unitless number
SL_T^0	Topographic surface constructed from L_T^0 columns plus elevation of top of blanket (ETB)	Meters (elevation)
$SL_{T,\alpha}$	Topographic surface constructed from $L_{T,\alpha}$ columns plus ETB	Meters (elevation)
V_α	Former volume percent sulfides, estimated by volume of indigenous limonite voids	cm^3
X_{Cu}	Multiplication factor to convert V_α to b_α; based on sulfide stoichiometries and specific gravities (see Table 1)	Percent copper per cm^3
z	Depth	Meters
z_R	Depth of redox boundary; progress variable for supergene enrichment process under conditions of descending water table	Meters
$\left(\frac{\partial b_\alpha}{\partial z}\right)_{x,y,z}$	Rate of change of reconstructed blanket grade with depth in present leached capping; subscripted parameters (x, y, z) held constant	Percent metal per meter
$\left(\frac{\partial b}{\partial z_R}\right)_{x,y,z}$	Rate of change of former metal grade in enriched zone with progress variable (depth of redox boundary); subscripted parameters (x, y, z) held constant	Percent metal per meter
ρ_b	Average rock density of enrichment blanket	Grams rock per cm^3
ρ_l	Average rock density of leached capping	Grams rock per cm^3
ρ_p	Average rock density of protore	Grams rock per cm^3

changes were observed in lithology, alteration mineralogy, or limonite characteristics. Where outcrops were unavailable, the top portions (generally 60 m) of diamond drill holes were used. Midpoint locations of the composite samples are shown in Figure 4. Composite samples were prepared for analysis using 500 g of each hand sample where available. Samples were analyzed by powder X-ray diffraction (XRD; Fig. 4) and various geochemical techniques, the results of which will be presented elsewhere.

Estimation of $(py/cc)_\alpha$ for each sample was based on the empirical correlations summarized in Table 1

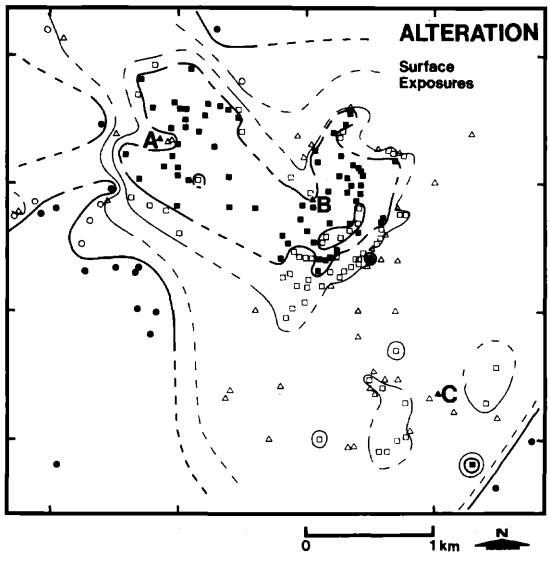

FIG. 4. Alteration mineralogy of surface exposures at La Escondida, based on semiquantitative interpretation of powder X-ray diffraction (XRD) data for more than 200 composite samples from roadcuts, trenches, and the upper portions of diamond drill cores. Each symbol on the map denotes a composite sample, as described in text. Open symbols = presence of greater than trace amounts of sericite; solid squares = advanced argillic-abundant pyrophyllite with locally abundant alunite, diaspore, and kaolinite; open squares = phyllic-advanced argillic-sericite and pyrophyllite both moderately abundant, with locally abundant alunite, kaolinite, and diaspore; open triangles = phyllic-abundant sericite, with locally abundant kaolinite; open circles = phyllic-potassic-fresh–both sericite and feldspar (plagioclase and/or K-feldspar) moderately abundant, with locally abundant chlorite and biotite; solid circles = potassic-propylitic-fresh–abundant feldspar(s), with biotite, chlorite, and/or epidote; solid triangles = summits of hills A, B, and C, at elevations 3,436, 3,355, and 3,194 m above sea level, respectively.

and Figure 1. The former sulfide volume V_α was determined by visual comparison with standard charts for each individual hand sample and then averaged with other samples in the group to yield the composite value. For each composite sample, the relative abundance and Munsell color of the six most common limonite minerals or mineral mixtures were logged, with attention to mode of occurrence (indigenous vs. transported), texture, and mineralogy. Mineralogical identification of limonites was based on dry scratch color, using a Munsell Soil Color Chart (Munsell Color Company, 1975) and data supplied by Loghry (1972). Results of XRD analysis of several dozen limonite separates shows good agreement with color data for limonite minerals from several southwestern U.S. porphyry deposits (Loghry, 1972) and other sources (e.g., Torrent et al., 1980). La Escondida hematites show Munsell scratch colors in the narrow range of 10R 4/6 to 10R 5/8. Dilution by gypsum or silica causes an increase along the value color axis, to colors such as 10R 4/10. La Escondida jarosites have scratch colors ranging from 2.5Y 8/6 to 5Y 8/10. Pure goethites show scratch colors close to 10YR 6/8. La Escondida goethites appear to be quite low in diaspore component (<4 mole % AlOOH), based on analysis of XRD peak positions (Schulze, 1984). Scratch colors between Munsell hues 7.5YR and 2.5YR were interpreted to consist of mixtures of hematite and goethite, with or without jarosite, as confirmed by XRD analysis of several samples.

Reconstructed copper-grade estimates were made without knowledge of sample location, to ensure objectivity. This is quite a different procedure from traditional surface mapping, where geologic features are mentally integrated, in many cases subjectively, to fit evolving patterns and models of a structural nature. In this sense, the approach to surface mapping taken here is akin to a geochemical sampling program, where the determination of $(py/cc)_\alpha$, V_α, and b_α are objective analytical results analogous to assays. Overall uncertainty in estimates of b_α may be as high as ±30 percent of the amount of copper formerly present; the main contributor to this uncertainty is probably the volume term.

Alteration and Sulfide Mineralization

An introduction to the lithology, alteration, and mineralization of the porphyry copper deposit at La Escondida, Chile, was provided by Brimhall et al. (1985). In that study, principles of mass balance were applied to vertical profiles of copper grade and rock density to deduce the magnitude and probable directions of lateral supergene copper fluxes. The geochronology of hypogene and supergene alteration and the erosional history at La Escondida are described by Alpers (1986) and Alpers and Brimhall (1988). Additional detail regarding the paragenesis of hypogene sulfide veins in the district is given by Alcayaga (1984). In this section, we present mineralogic data concerning the distribution of hypogene and supergene wall-rock alteration and sulfide mineralization at La Escondida as necessary background to interpretation of dominant chemical and hydrologic controls on supergene metal transport.

Hypogene alteration

Mineralogic data from semiquantitative XRD studies of several hundred surface and downhole composite samples are summarized in Figure 4. Subsurface alteration data along a north-south cross section are given by Alpers and Brimhall (1988). A significant correlation is displayed at La Escondida between hypogene alteration mineralogy and mobility of copper in the supergene environment (Brimhall et al., 1985), as is typically observed in porphyry copper deposits (McClave, 1973; Titley, 1982).

Potassic alteration is manifested differently in the

different wall rocks at La Escondida. Pervasive biotitization and K-feldspar veining characterize an andesitic unit, which is exposed at the surface in the southwestern and extreme northern portions of the district (Fig. 4; also refer to geologic map and cross section by Alpers and Brimhall, 1988). Within the porphyritic intrusions in the southeast zone (between hills B and C), veins of potassium feldspar, anhydrite, quartz, and biotite are preserved locally beneath the zone of intense phyllic alteration (and deepest supergene alteration). A transition zone of mixed phyllic-potassic alteration with both sericite and feldspar, plus chlorite after biotite separates the potassic zone from the phyllic zone throughout the district. In Figure 4, this mixed phyllic-potassic alteration assemblage is lumped together with relatively fresh rocks which contain sericite and unaltered feldspar to make up a zone labeled "phyllic-potassic-fresh." Although it is possible that some of the sericite is of supergene origin, a hypogene origin is most consistent with radiometric age data (Alpers and Brimhall, 1988) and stable isotope data (Bird, 1988).

Propylitic alteration characterized by epidote, chlorite, and calcite is found in fringe areas (generally beyond the area shown in Fig. 4), apparently gradational and contemporaneous with the potassic alteration. Geologic observations and radiometric dating of hypogene alteration minerals from La Escondida (Alpers, 1986; Alpers and Brimhall, 1988) are consistent with the model of Rose (1970) and others (e.g., Beane and Titley, 1981) who envision an early propylitic fringe surrounding the potassic zone, with later zones of phyllic and advanced argillic alteration superimposed on this early pattern.

Phyllic alteration is defined for this study by the presence of abundant sericite without significant prophyllite or feldspar. The phyllic zone dominates the central portion of the district (Fig. 4) and extends to the northwestern part of the district along a deep trough controlled by fault structures with possible syn- and posthypogene fault displacements.

Advanced argillic alteration at La Escondida is characterized by abundant pyrophyllite, with locally abundant diaspore, alunite, and svanbergite (Stoffregen and Alpers, 1987) and with no more than trace amounts of sericite. At the scale of the composite samples, the pervasive advanced argillic assemblage is found only in the area of hills A and B (Fig. 4). A mixed zone of advanced argillic-phyllic alteration, in which pyrophyllite and sericite are both moderately abundant in whole-rock samples, separates the advanced argillic and phyllic zones (Fig. 4). The strong inverse correlation between sericite and pyrophyllite abundance in the mixed phyllic-argillic zone suggests that the advanced argillic alteration was superimposed on a preexisting phyllic zone (cf. Gustafson and Hunt, 1975); however, there are no direct petrographic observations to support this interpretation. Silicification accompanying advanced argillic alteration probably accounts for the preservation of these areas as hills. This topography may have been an important contributing factor to lateral fluxes of copper away from these hills during supergene enrichment at a time when the climate was significantly wetter (Alpers et al., 1984; Brimhall et al., 1985; Alpers and Brimhall, 1988).

Supergene alteration

Mineralogical effects caused by supergene alteration of gangue minerals include the destruction of feldspars, chlorite, biotite, and anhydrite and the deposition of supergene kaolinite, gypsum, and alunite. Supergene kaolinite is rare or absent in zones of pervasive advanced argillic alteration and mixed phyllic-advanced argillic assemblages, but it tends to increase in abundance with depth in the phyllic and mixed phyllic-potassic(-fresh) zones. This distribution pattern probably corresponds to the former distribution of feldspars and other minerals (biotite and chlorite) which kaolinite has replaced; however, there is only limited petrographic evidence because of the texture-destructive nature of the supergene alteration and the locally intense (hypogene) brecciation.

Supergene kaolinite alteration and dissolution of hypogene anhydrite extends to depths well below the base of strong copper enrichment, to a zone defined as the quasi-protore (Brimhall et al., 1985). In general, the quasi-protore is a zone which has experienced minimal supergene metal enrichment, but which exhibits measurable changes in mineralogy and bulk physical properties (reduced density and increased porosity) due to supergene alteration (Cunningham, 1984).

Supergene alunite occurs as cryptocrystalline veins and fracture coatings up to 1 cm in width and as fine-grained disseminations throughout the phyllic and advanced argillic alteration zones. Preliminary distinctions between supergene and hypogene alunite based on grain size and color have been confirmed by sulfur isotope analysis and K-Ar dating (Alpers and Brimhall, 1988). The spatial distribution of supergene alunite extends to depths of at least 50 m below the elevation of the present top of the sulfides, in contrast with supergene kaolinite, which extends to several hundred meters depth below the present top of the sulfides. Supergene alunite in the leached capping zone has been extensively replaced by jarosite ($FeAl_{-1}$ exchange), the iron made available by pyrite oxidation.

Hypogene sulfide mineralization

It is possible to outline only the most general features of districtwide hypogene sulfide zoning at La Escondida because most diamond drill holes at La Escondida did not go through the zone of incipient

copper enrichment into true protore or quasi-protore rocks (Brimhall et al., 1985). In general, the district-wide sulfide zoning correlates well with patterns of hypogene wall-rock alteration. The fringe areas, in zones of propylitic and weak potassic alteration, are characterized by a pyritic protore with traces of chalcopyrite and relatively low hypogene copper grades. Moving inward toward zones of phyllic and mixed phyllic-potassic alteration, chalcopyrite becomes more abundant relative to pyrite in protore sulfides and traces of bornite appear. Bornite abundance reaches a maximum in several relatively small pockets low in pyrite, generally associated with potassic alteration overprinted by phyllic alteration. The bornite-chalcopyrite zones are areas of maximum protore copper grade and represent the most central part of the hypogene sulfide zoning pattern, as presently exposed.

Many other porphyry copper deposits show a similar overall sulfide zoning pattern: an innermost chalcopyrite-bornite zone with low pyrite, grading outward (and upward?) to a chalcopyrite-pyrite zone and then an outermost pyritic fringe (e.g., El Salvador, Chile, Gustafson and Hunt, 1975; Bethlehem, British Columbia, Briskey and Bellamy, 1976). There is no barren core of low total sulfides and abundant Fe-Ti oxides recognized at La Escondida at the present depth of exploration, in contrast to the hypogene mineralization zoning at numerous other porphyry-type deposits, including El Salvador, Chile (Gustafson and Hunt, 1975), Bingham, Utah (James, 1971), and Kalamazoo, Arizona (Lowell, 1968). This is one of several factors which suggest that only the higher levels of the mineralized system have been exposed. Minor amounts of magnetite are present in the bornite-chalcopyrite zone at La Escondida, and significant amounts of magnetite are present in the zone of potassic alteration affecting the andesitic unit exposed in the southwestern portion of the district (Fig. 4).

Petrographic study of relict sulfides in polished sections of leached capping samples from La Escondida (Minera Utah de Chile, unpub. data) indicates that the original hypogene sulfide zoning now observed at the level of the present surface is similar to that observed at depth. One exception to the apparent vertical continuity of hypogene sulfide zoning is the northeastern part of the district (hill B, Fig. 4) where the rhyolitic porphyry contains relict sulfides composed mostly of pyrite, despite the presence of relatively high-grade bornite-chalcopyrite and pyrite-chalcopyrite protore at depth in that area. The relatively high original pyrite content of the rhyolitic porphyry contributed an abundant supply of sulfuric acid during weathering, which facilitated leaching of adjacent and underlying rocks (Brimhall et al., 1985). Crosscutting relations and radiometric age determinations (Alpers and Brimhall, 1988) suggest that the rhyolitic porphyry as well as several late dikes of quartz latitic composition were intruded after the main period of hypogene copper mineralization.

Minor amounts of coarse-grained covellite of probable hypogene origin are observed locally in narrow (<1 cm wide) veinlets in the present sulfide zone in association with advanced argillic alteration. Hypogene covellite, chalcocite, enargite, and tennantite are observed only rarely in relict sulfides trapped in quartz in the leached capping of the northwestern portion of the district (hill A, Fig. 4). In general, relict sulfides preserved in the leached capping zones of porphyry copper deposits represent early hypogene sulfides protected not only from supergene oxidation and/or enrichment but also from late hypogene sulfidation effects (Gustafson and Hunt, 1975; Brimhall and Ghiorso, 1983). Thus, these late sulfides, indicative of relatively high f_{S_2} conditions, may have been originally more abundant at La Escondida in places unprotected from either late hypogene sulfidation or supergene oxidation effects.

Supergene sulfide mineralization

The replacement of hypogene copper-iron sulfides by supergene copper sulfides represents the economically critical step in the supergene enrichment of copper grades to mineable levels. Inorganic sulfate reduction in the subsurface is exceedingly slow at low temperatures (Ohmoto and Lasaga, 1982), so the principal source of sulfur in the supergene sulfides is probably the hypogene sulfides (Field and Gustafson, 1976), although massive chalcocite at the extreme top of the enrichment blanket may represent a thin zone of bacterially mediated sulfate reduction. Quantitative modal data for copper sulfide minerals from a representative vertical diamond drill hole at La Escondida are shown in Figure 5. Samples were prepared by concentration of heavy minerals using heavy liquids (sp gr > 2.96 g/cm^3). Modal line counting was performed using automated rock analysis techniques (Brimhall, 1979; Brimhall and Rivers, 1985).

Digenite(-anilite) was distinguished from chalcocite(-djurleite) by its sky-blue color in reflected light and its lower Cu/S ratio from electron microprobe analysis. The phase referred to here as supergene digenite(-anilite) may actually consist of digenite, anilite, or a mixture of the two phases. Digenite and anilite have nearly identical optical properties and composition and can be distinguished only by careful XRD without grinding, which can convert anilite to digenite (Clark and Sillitoe, 1971). In this paper, we refer to the sky-blue, isotropic phase(s) of the ideal composition $Cu_{1.70\text{-}1.74}Fe_{0.05\text{-}0.01}S$ as digenite(-anilite), although the exact mineralogy and composition of this phase remains undetermined.

The upper portion of the zone of strong copper enrichment (Brimhall et al., 1985) is dominated by whitish-gray massive chalcocite (Sillitoe and Clark,

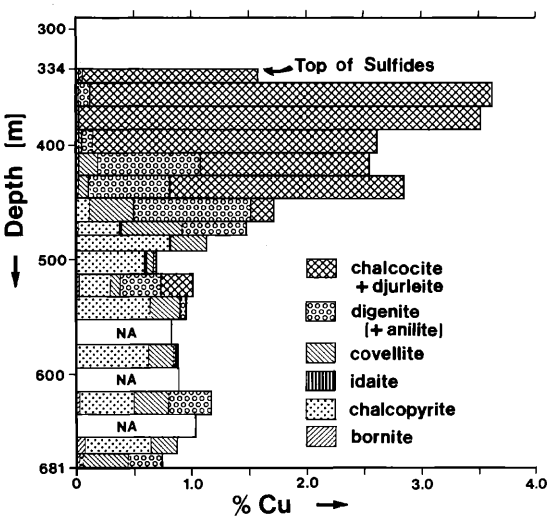

FIG. 5. Vertical profile of copper(-iron) sulfide mineralogy in diamond drill hole 219 (location shown in Fig. 8). Areas proportional to copper contribution from each mineral. Sulfide mineralogy determined by reflected light microscopy supplemented by electron microprobe analysis. Data gathered on heavy mineral separates from continuous downhole composite samples using automated line-counting methods (Brimhall, 1979; Brimhall and Rivers, 1985). NA = not analyzed.

1969) which probably consists of a fine-grained mixture of djurleite ($Cu_{1.934\text{-}1.965}S$) and low chalcocite ($Cu_{1.995\text{-}2.000}S$) based on semiquantitative electron microprobe analysis (formulas from Potter, 1977). Traces of hypogene chalcopyrite, bornite, and digenite were shielded from supergene replacement and persist in the zone of strong enrichment as less than 10-μm-diam inclusions in pyrite grains. In these inclusions, digenite is invariably associated with bornite and probably represents an exsolution product. In the zone of strong enrichment, chalcocite(-djurleite) has replaced virtually all hypogene chalcopyrite and bornite as well as some of the pyrite. Toward the bottom of the zone of strong enrichment, the abundance of supergene digenite(-anilite) increases and chalcocite(-djurleite) rims on pyrite grains decrease in thickness. In the zone of incipient enrichment, covellite is the dominant supergene sulfide with traces of digenite(-anilite) and chalcocite(-djurleite). Minor amounts of idaite (Cu_3FeS_4) are associated with fine-grained covellite and chalcopyrite and are considered to represent a supergene replacement of bornite (cf. Sillitoe and Clark, 1969).

The modal pyrite content of the vertical profiles shows a variable distribution due to the presence of pyritic veins. This variability makes it impossible to document any systematic depletion of pyrite near the tops of the sulfide profiles, a relationship expected from the textural observation that chalcocite has replaced pyrite extensively in the upper portion of the zone of strong enrichment.

It is clear from detailed counting of sulfide assemblages in composite profiles from several vertical diamond drill holes that the sulfide mineralogy in the upper portion of the zone of strong copper enrichment can be approximated by the assemblage supergene chalcocite plus residual hypogene pyrite. This simplification provides a basis for the quantitative interpretation of limonites in the leached capping zone using the techniques described in the previous section.

The overall, large-scale reaction sequence of chalcopyrite → covellite → digenite(-anilite) → djurleite(-chalcocite) with increasing elevation (Fig. 5) can be explained most simply by an increasing oxidation potential within the stability field of $(SO_4^{-2})_{aq}$. Analysis of natural waters in oxidizing sulfide systems has shown that these waters are sulfate dominated (Sato, 1960; Thornber, 1975; Nordstrom, 1977; Sangameshwar and Barnes, 1983; Alpers, unpub. data). On a pE-pH diagram for the Cu-S-O-H system at 25°C and 1 bar (Fig. 6), it can be seen that this sequence is traversed with increasing oxidation potential or increasing pH in the sulfate field. Although aqueous SO_4 and H_2S do not equilibrate rapidly at low temperatures, Figure 6 still affords a useful representation of the reaction sequence, because aqueous H_2S activity decreases with increasing pE. The vertical zoning of supergene copper sulfides at La Escondida, in particular, the digenite(-anilite) zone, either is not well developed in other copper deposits or has gone largely unrecognized. Previous discussions of copper sulfide stability within oxidized and enriched deposits (e.g., Garrels, 1954; Garrels and Christ, 1965; Sillitoe and Clark, 1969; Anderson, 1982) make no reference to the above zoning pattern in vertical supergene profiles, which may be a function of the lack of drilling to sufficient depths in some mining districts because of economic constraints. Some notable exceptions are the description of a similar copper sulfide sequence in the supergene-enrichment zone of the Musoshi stratiform copper deposit, Zaire (Cailteux, 1974), the reported occurrence of digenite near the base of the enrichment blanket at Chuquicamata, Chile (Ambrus, 1979, 1980), and the observation of a hexagonal phase of composition $Cu_{1.83}S$ in the enrichment blanket zone at El Teniente, Chile (Clark, 1972). The above sequence of minerals has also been noted in low-temperature sediment-hosted strata-bound copper deposits (Ripley et al., 1980; Gablina, 1984), where the presence of djurleite indicates temperatures of formation below 93°C (Roseboom, 1966; Potter, 1977). The presence of a deep zone of incipient covellite enrichment beneath the chalcocite enrichment blanket has been noted briefly by previous workers (e.g., Bateman, 1950; Ambrus, 1979, 1980; Sillitoe et al., 1984) but has received little geochemical interpretation in the literature. In well-enriched deposits such as La Escondida and Chuquicamata, the recognition

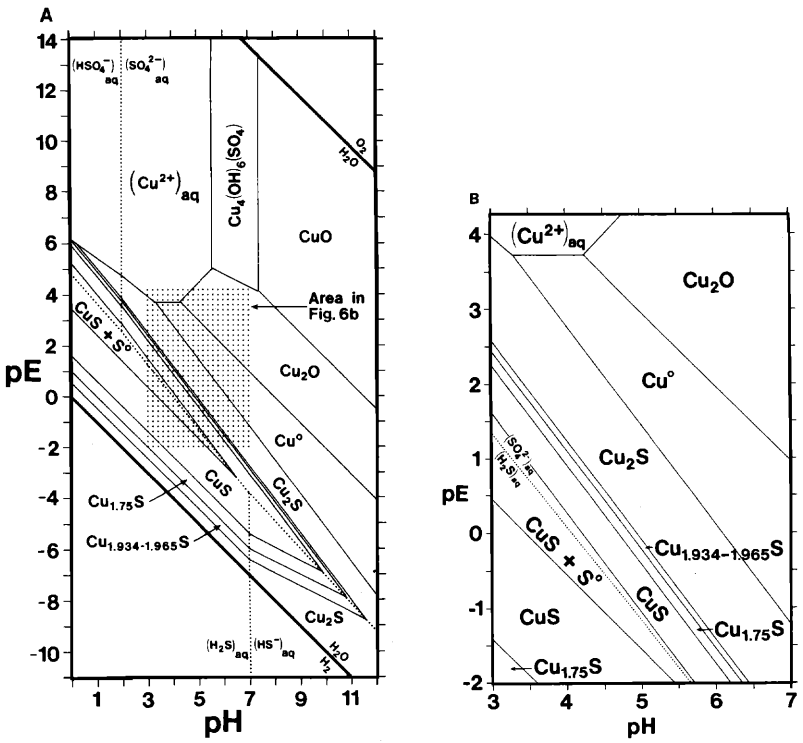

FIG. 6. A. pE-pH diagram for the Cu-S-O-H system at 25°C, 1 bar, with the activities of total aqueous sulfur at 10^{-2} and total aqueous copper at 10^{-4}; dotted lines denote equal activity of aqueous sulfur species. Thermodynamic data and sources are listed in Appendix I. B. Enlargement of shaded portion of A.

of a digenite(-anilite) zone may be useful for mine planning and grade control during mining, because the occurrence of digenite(-anilite) overlies the bottom of strong enrichment by several tens of meters.

Known occurrences of covellite and blaubleibender covellite at higher elevations than the chalcocite zone are probably examples of metastable transition phases formed during oxidation of previously formed chalcocite, djurleite, and/or digenite enrichment zones (Sillitoe and Clark, 1969; Marcantonio, 1976; Goble, 1981; Maynard, 1983). Such an upper zone of covellite was not observed at La Escondida, an observation consistent with the chalcocite enrichment blanket having been preserved by a rising water table, which contributed to the cessation of active supergene enrichment at La Escondida during the middle Miocene (Alpers et al., 1984; Alpers and Brimhall, 1988).

Results of Leached Capping Interpretation

Surface exposures

A quantitative map of supergene limonites in surface exposures at La Escondida is presented in Figure 7, interpreted in terms of the sulfide mineralogy prior to oxidation expressed as the $(py/cc)_\alpha$ ratio. The most striking feature of this map is the regularly concentric nature of the contour pattern for more than 200 composite samples (locations shown in Fig. 4). The jarositic zone at the margins of the district, interpreted in terms of $(py/cc)_\alpha$ ratio values greater than or equal to 7:1, provides evidence for a pyritic fringe, a hypogene feature typical of porphyry copper systems (Rose, 1970; Lowell and Guilbert, 1970; Gustafson and Hunt, 1975). Moving inward from the pyritic fringe zone, the $(py/cc)_\alpha$ ratio decreases systematically to minimum values less than 3:1 scattered throughout the central portion of the district in a roughly northwest-southeast trend.

Estimates of reconstructed preoxidation enrichment blanket grades, b_α, in present surface exposures (Fig. 8) show a roughly concentric pattern similar to the reconstructed preoxidation mineralogy (Fig. 7). The similarity of Figures 7 and 8 is testimony to the fact that the V_α distribution does not show any systematic or easily contourable variations throughout the district. It should be kept in mind during inspection of Figures 7 and 8 that the present topographic surface where these mapping data were collected does not represent a single former enrichment blanket, but rather, a composite of former enriched zones from different stages during the supergene evolution of the deposit which are exposed at the present surface due to differential erosion. Higher elevations in the leached capping can generally be taken to represent

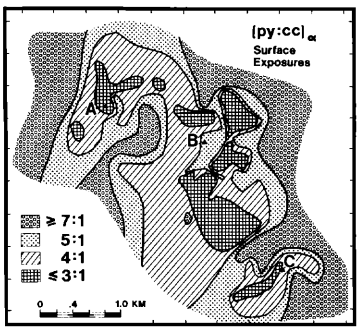

FIG. 7. Reconstructed pyrite chalcocite ratio, $(py/cc)_\alpha$, for surface exposures, using methods described in text and correlations summarized in Figure 1 and Table 1. Location of composite sample midpoints shown in Figure 4.

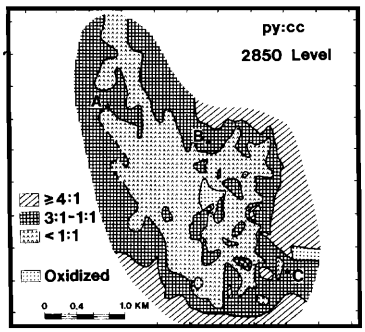

FIG. 9. Present sulfide mineralogy, 2850 level (elevation in meters above sea level). Pyrite chalcocite ratio (py/cc) based on macroscopic core logging and underground mapping (Minera Utah de Chile, unpub. data).

earlier stages in the supergene history of the deposit. In the central areas of Figures 7 and 8 near hills A and B, the surface exposures are up to 350 m above the present top of sulfides. The extreme thickness of leached capping in these areas has preserved the evidence for relatively weak, incipient copper sulfide enrichment near the present surface, which formed at relatively early stages of supergene evolution in the district. (See Brimhall et al., 1985, fig. 19A and B for topographic contour maps of surface elevation and the elevation of the top of the copper sulfide enrichment blanket.)

It is useful to compare the results of limonite interpretation in surface exposures with the actual sulfide mineralogy and copper grade of the present underlying copper sulfide enrichment blanket. The distribution of the present py/cc ratio and present copper grades on the 2850 level are shown in Figures 9 and 10, respectively. The pyritic halo can be recognized in Figure 9, although the data are limited to a smaller portion of the district than in Figures 7 and 8. Comparison of the data in Figures 7 and 9 shows that py/cc ratios at a given location in the present chalcocite blanket zone (Fig. 9) tend to be significantly lower than the reconstructed $(py/cc)_\alpha$ at the top of the present leached capping zone. This difference may be due to a combination of both hypogene and supergene sulfide zoning effects. A decreasing hypogene pyrite/chalcopyrite ratio with depth could account for this difference; supergene effects such as progressively more complete replacement of pyrite by chalcocite with descent of the enriched zone through the rock column may also have been important, although this effect is difficult to quantify because of variability in the pyrite content. Petrographic evidence for supergene replacement of pyrite by chalcocite is abundant in samples from throughout the zone of strong enrichment at La Escondida, indicative of the mature nature of the sulfide enrichment process (Titley, 1982).

There is also a significant difference between the copper grade of the present enrichment blanket and that of the reconstructed former enrichment blanket(s) at the present surface. The reconstructed blanket at the present surface (Fig. 8) has zones of maximum grade (>1.5% Cu) in several restricted zones with a total areal extent of less than 0.2 km^2, whereas the present enrichment blanket at the 2850 level (Fig.

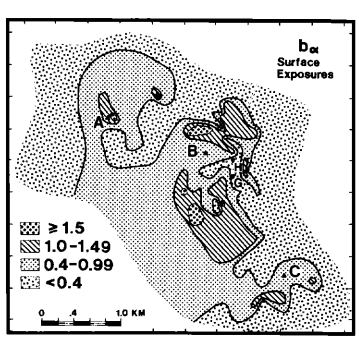

FIG. 8. Reconstructed former enriched zone copper grade, b_α, for surface exposures. Location of diamond drill holes 219 and 176 shown as points G and H, respectively.

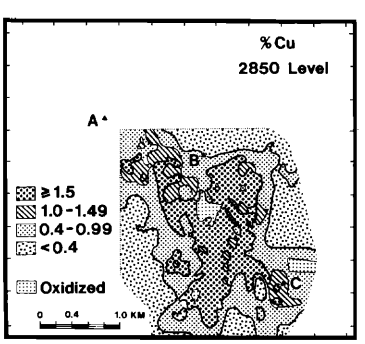

FIG. 10. Present copper grade, 2850 level. Based on geologic ore reserve (Minera Utah de Chile, unpub. data). Grade regions are not necessarily concentric.

10) averages >1.5 percent Cu over more than 2.0 km^2. The dramatic increase in enriched copper grade from the zones of former enrichment at the present surface to the present sulfide enrichment blanket is attributed to the phenomenon of cumulative downward enrichment. First proposed by Locke (1926) and mentioned by others (Bateman, 1950; Ambrus, 1979; Titley, 1982; Anderson, 1982) as an intuitive likelihood, progressive cumulative enrichment results from the long-term descent of the oxidation-reduction (redox) front through the rock column, allowing the enriched zone at the top of the reduced zone to accumulate protore copper progressively as the redox front descends (Brimhall et al., 1985).

The actual location of the redox front is not precisely at the water table per se, but rather, at the top of the capillary fringe, a zone where water pressure is less than atmospheric, yet pores are full of water by capillary suction (Freeze and Cherry, 1979). The detailed geometry and thickness of the capillary fringe zone remains poorly documented in fractured-rock systems, however; for simplicity, we refer to the redox front and water table interchangeably.

The cumulative enrichment effect will only be realized in systems where rates of sulfide oxidation and water infiltration are able to keep pace with rates of erosion and water table descent. As a supergene enrichment system evolves, both the grade and thickness of the enrichment blanket may increase as a function of time and depth, depending on factors discussed by Brimhall et al. (1985) and below. In the next section, results of quantitative limonite mapping in vertical profiles at La Escondida are used to document the cumulative downward enrichment effect and to verify the calibration of the quantitative mapping techniques used in this study.

Vertical profiles

Vertical profiles of actual copper grades in enriched profiles (Figs. 5, 11, and 12) show maximum copper grades near the top of sulfides in the uppermost portion of the zone of strong enrichment. Assuming the net downward movement with time of the redox front, it seems reasonable to conclude that b_α determined from the oxidation products within a given volume of enriched rock represents the maximum enriched copper grade attained by that volume of rock prior to oxidation.

Quantitative limonite mapping and copper-grade reconstruction were carried out for 13 vertical diamond drill holes; representative results from two of these profiles are shown in Figures 11 and 12 (locations in Fig. 8). Core logging was carried out in continuous composite intervals of 20 m or less where macroscopic changes in alteration, lithology, or limonite characteristics were encountered.

In all 13 leached capping profiles examined in detail, the estimated former blanket grade (b_α) was found to increase systematically with depth, as illustrated in Figures 11 and 12. The reconstructed preoxidation sulfide mineralogy, expressed as the $(py/cc)_\alpha$ ratio, was also found to change toward less pyritic values, which can be attributed to both hypogene and supergene zoning effects, as discussed above. Estimated values of b_α and $(py/cc)_\alpha$ near the base of the leached capping zone are in reasonable agreement with actual copper grades and py/cc values in the upper portion of the present enrichment blanket, as determined by atomic absorption assays, macroscopic core logging, and microscopic modal analysis of heavy mineral separates prepared from composite assay pulps (e.g., Fig. 5).

The relatively continuous increase of b_α with depth in Figures 11 and 12 indicates that the redox front dropped in a relatively continuous manner, for the most part by increments of distance less than the composite mapping interval of 20 m. Local maxima in b_α may represent elevations where the redox front resided for a relatively long time and from which there was a relatively catastrophic drop in redox front elevation by a vertical distance greater than the mapping

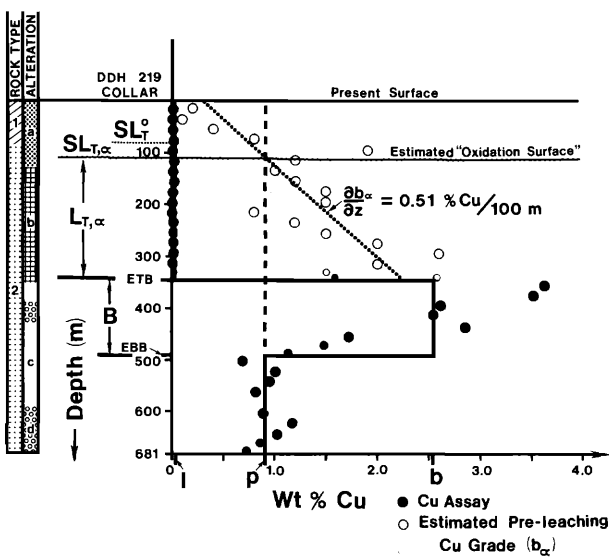

FIG. 11. Vertical profiles of estimated former enriched zone copper grade in leached capping, b_α (open circles) vs. depth for diamond drill hole 219. Location of drill hole indicated in Figure 8. Actual copper grades (determined by atomic absorption) for continuous composite samples shown in solid circles. Diameter of circles proportional to composite sample length (8–20 m). Dotted line represents result of linear least squares regression for b_α vs. depth (z): $b_\alpha = 0.0051(z) + 0.375$; $n = 17$, $r^2 = 0.58$. Rock types: (1) rhyolitic porphyry and (2) Escondida porphyry (quartz monzonite?), described by Alpers (1986). Alteration types: (a) advanced argillic, (b) phyllic-advanced argillic, (c) phyllic, (d) phyllic-potassic(-fresh), as described in Figure 4 caption. Symbols ETB and EBB are explained in Table 3 and text.

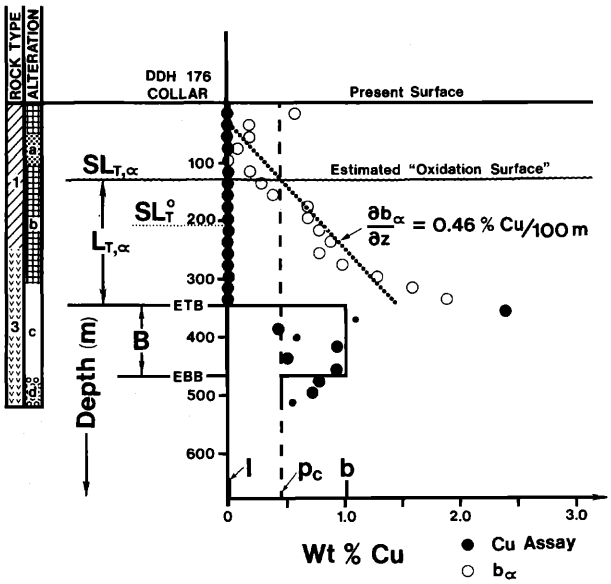

FIG. 12. Same as Figure 11, for diamond drill hole 176. Location is indicated in Figure 8. Result of linear least squares regression for b_α vs. depth (z): $b_\alpha = 0.0046(z) - 0.139$; $n = 17$, $r^2 = 0.76$.

interval. The thickness of the enriched zone prior to relatively sudden water table descent must have been at least 60 m, because limonite mineralogy and textures indicate oxidation of a pyrite-chalcocite assemblage of copper grade greater than protore; no angular goethitic boxworks indicative of chalcopyrite oxidation (Blanchard, 1968) were observed. Therefore, it appears that the water table did not drop far enough to expose unenriched protore sulfides to oxidation after the very initial stages of enrichment, the record of which is preserved only sporadically at the present surface (J. H. Courtright, pers. commun., 1983).

The mapping of diamond drill core from vertical holes in leached capping can therefore provide quantitative evidence for cumulative enrichment of the chalcocite zone as it descended through the rock column. The changing elevation of the redox boundary can be considered as a progress variable for the supergene enrichment process, acting essentially as a proxy for time as the water table descended through the rock column, exposing new volumes of sulfides to conditions of oxidative weathering. The reconstructed parameters $(py/cc)_\alpha$ and b_α represent approximations for the former sulfide mineralogy and total copper grade, respectively, of the sulfide-bearing rocks immediately prior to oxidation, taking into account implicitly any cumulative effects of enrichment prior to oxidation. Thus, in a well-preserved supergene system, information concerning the copper grade and mineralogy of formerly enriched zones is stored by the residual limonite minerals of characteristic texture and mineralogy in the leached capping zone. It is necessary to decipher this record in order to understand the dynamic chemical evolution of the supergene enrichment system.

Geochemical Dynamics of Supergene Enrichment Systems

In general, only descending or steady-state ground-water table conditions are favorable to supergene copper sulfide enrichment (Bateman, 1950; Brimhall et al., 1985). If the ground-water table ascends and saturates the zone of oxidative leaching, this can lead to the depletion of dissolved oxygen and ferric iron, resulting in the cessation of sulfide oxidation and precluding further downward copper transport. The descent of the ground-water table need not be continuous in time; temporary ascent of the ground-water table, or a time interval without significant water infiltration, would cause temporary cessation of supergene reaction progress, which would become reactivated upon further ground-water table descent or water infiltration (Bladh, 1982).

In the following section, analytical expressions derived by Brimhall et al. (1985) for mass balance in weathering profiles are combined with observations from La Escondida to derive two contrasting models for the dynamic geochemical evolution of supergene enrichment systems under conditions of a descending water table.

Mass balance considerations

Brimhall et al. (1985) derived the following expression for mass balance in vertical weathering profiles:

$$B(b\rho_b - p\rho_p) = L_T(p\rho_p - l\rho_l) + \text{flux}, \qquad (2)$$

where l, b, and p represent average metal grades in leached capping, enrichment blanket, and protore zones, respectively; ρ_l, ρ_b, and ρ_p denote the average bulk density of the subscripted zones (in g/cm^3); B represents the thickness (m) of the enriched zone; L_T represents the total thickness of the leached capping zone, including eroded material; and flux refers to lateral fluxes of metal (in g/cm^2) either into or out of the volume of rock represented by the vertical profile or drill hole. For a closed system where flux = 0, this equation reduces to:

$$B(b\rho_b - p\rho_p) = L^0_T(p\rho_p - l\rho_l), \qquad (3)$$

where L^0_T denotes total leached column height assuming no lateral flux. Rearranging eq. (3) to solve for b yields:

$$b = \underset{(1)}{\frac{p\rho_p}{\rho_b}} + \underset{(2)}{\left(\frac{L^0_T}{B}\right)} \underset{(3)}{\left(\frac{p\rho_p - l\rho_l}{\rho_b}\right)}, \qquad (4)$$

an expression which can be used as a framework for describing the interrelationships of metal grades, bulk densities, and zone thicknesses in an evolving supergene system (Brimhall et al., 1985).

If term (2) and either term (3) or (4) are assumed to remain constant with time, then eq. (4) reduces to the equation for a straight line. Holding terms (2) and (3) constant implies that blanket thickness increases in direct proportion to the total cumulative thickness of the leached zone, whereas holding terms (2) and (4) constant implies that leached zone grade stays constant through time. These alternative sets of assumptions form the basis for the models described in detail below.

Under conditions of a descending water table, the elevation of the redox front, z_R, can be thought of as the progress variable for the cumulative enrichment process. Based on reconstructed profiles of b_α vs. depth (Figs. 11 and 12), we stipulate for the purpose of the following simplified models that average enrichment blanket grade increases as a linear function of the progress variable, z_R, during evolution of the supergene enrichment system. In the following discussion, we explore the algebraic implications of this assumption in the context of two contrasting analytical models for supergene profile evolution. The paleohydrologic implications of these models are then evaluated by comparison of the analytical expressions with field data from La Escondida.

Increasing blanket thickness (IBT) model

In the increasing blanket thickness model, we hold the quotient $\frac{L_T^0}{B}$ constant for all values of z_R, which implies that the enrichment blanket thickness, B, grows linearly in proportion to the total cumulative leached column height, L_T^0. Protore grade, p, and all density terms are also assumed to remain constant with respect to the progress variable, z_R. Insufficient drilling data are available to define vertical variations in protore grade at La Escondida; however, lateral variations in protore grade are accounted for because a different value of p is computed for each drill hole. Average bulk densities of oxidized, enriched, and protore zones at La Escondida are 2.42, 2.53, and 2.57 g/cm^3, respectively. Treating each of the density variables as a constant during evolution of the weathering profile is a reasonable simplifying assumption.

In the increasing blanket thickness model, the rate of water table descent is relatively rapid with respect to the rate of sulfide oxidation and copper leaching. In this model, the average grade of the leached zone decreases continuously and the average blanket grade increases in response to the descending water table. This relationship is displayed graphically in Figure 13A and B for a schematic copper grade profile. A maximum blanket grade, b_{max}, is attained when the average leached zone grade reaches l_{min}, which can in practice be as low as 0.01 to 0.02 percent Cu (Figs. 11 and 12).

The derivative of eq. (4) with respect to z_R for the increasing blanket thickness model, holding the subscripted variables constant, is expressed by:

$$\left(\frac{\partial b}{\partial z_R}\right)_{IBT} \equiv \left(\frac{\partial b}{\partial z_R}\right)_{\frac{L_T^0}{B},p,\rho_l,\rho_b,\rho_p} = -\left(\frac{L_T^0}{B}\right)\left(\frac{\rho_l}{\rho_b}\right)\left(\frac{\partial l}{\partial z_R}\right)_{\frac{L_T^0}{B},p,\rho_l,\rho_b,\rho_p}. \quad (5)$$

By ignoring the density terms for the sake of simplicity, the algebraic relationship in eq. (5) can be interpreted graphically in Figure 13A and B. These diagrams show four stages in the evolution of the leached and enriched zones, showing the incremental progress of $z_{R,n}$ for (n = 1, 2, 3, . . . max). The symbols b_n, l_n, $L_{T,n}^0$, and B_n indicate that the variables b, l, L_T^0, and B are all functions of z_R. A comparison of the algebraic derivations and the graphical interpretation for Figure 13 is given in Appendix II.

Complete incremental leaching (CIL) model

An alternative interpretation of eq. (4) with significantly different implications for the manner of growth of the enriched zone as a function of the descent of the ground-water table is to allow term (3) in eq. (4), $\frac{L_T^0}{B}$, to change as a function of z_R, and to consider term (4) in eq. (4) to be constant. This case corresponds to a relatively rapid rate of sulfide oxidation relative to the rate of water table descent. After each incremental drop in the water table, essentially complete leaching is allowed to take place prior to the next incremental drop. For each increment of water table descent, the average leached zone grade approaches l_{min}, which is a function of rock type, alteration mineralogy, the effective Me/S ratio in sulfides, and the total sulfide content. As in the increasing blanket thickness model, the protore grade and the density terms remain constant with z_R in the complete incremental leaching model. Thus, with the subscripted constants, the partial derivative of b with respect to z_R from eq. (4) is expressed by:

$$\left(\frac{\partial b}{\partial z_R}\right)_{CIL} \equiv \left(\frac{\partial b}{\partial z_R}\right)_{p,l_{min},\rho_l,\rho_b,\rho_p} = \left(\frac{(p\rho_p - l_{min}\rho_l)}{\rho_b}\right)\left(\frac{1}{B} - \frac{L_T^0}{B^2}\left(\frac{\partial B}{\partial z_R}\right)_{p,l_{min},\rho_l,\rho_b,\rho_p}\right). \quad (6)$$

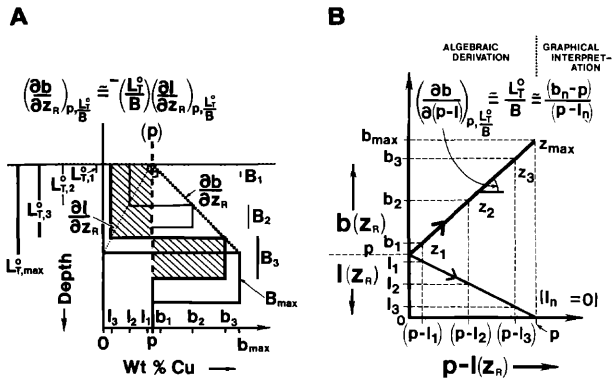

FIG. 13. Increasing blanket thickness model for dynamic evolution of supergene enrichment system. A. Schematic plot of copper grade vs. depth, showing enrichment blanket thickness, B_n, growing in direct proportion to total leached column height, $L^0_{T,n}$, at a constant ratio, $\frac{L^0_T}{B}$ with constant protore grade, p. Leaching becomes progressively more complete as the water table descends. Ruled areas ($n = 3$) are equal because of mass balance constraints, neglecting density terms for simplicity (see Appendix II). B. Schematic composite plot of $b(z_R)$ and $l(z_R)$ vs. $(p - l(z_R))$, with both b and l changing as functions of the progress variable, z_R, in direct proportion to the slope $\frac{L^0_T}{B}$, neglecting density terms.

The model represented by eq. (6) is nonlinear in terms of the predicted increase in average blanket grade, b, as a function of z_R and blanket thickness, B. However, this expression becomes linear if the simplifying assumption is made that the blanket thickness, B, does not change as a function of z_R, as shown below. In support of this assumption, consider that the depth of enrichment depends largely on the local hydrology, including such factors as the permeability of the various alteration zones, topographic relief, and rates of precipitation and infiltration, as well as on the kinetics of secondary mineral precipitation relative to the rate of ground-water flow in the lower portion of the blanket zone. It could be reasonably argued that the depth of circulation of meteoric waters is established relatively early in the evolution of a supergene system in response to the local hydrology (e.g., Mocoa, Colombia, Sillitoe et al., 1984). As a supergene system evolves, the enrichment blanket thickness could remain more or less constant if the other factors controlling the depth of enrichment remain in balance. In this scenario, copper picked up during redox front descent would contribute to an increase in the grade of the enrichment blanket but not to its thickness.

Thus, for a special case of the complete incremental leaching model in which the blanket thickness, B, remains constant as a function of z_R, $\left(\frac{\partial B}{\partial z_R}\right) = 0$, so that eq. (6) reduces to:

$$\left(\frac{\partial b}{\partial z_R}\right)_{CIL} \equiv \left(\frac{\partial b}{\partial z_R}\right)_{B,p,l_{min},\rho_l,\rho_b,\rho_p} = \left(\frac{p\rho_p - l_{min}\rho_l}{B\rho_b}\right). \quad (7)$$

The case represented by eq. (7) is illustrated graphically for a schematic grade profile in Figure 14A and B. See Appendix II for further derivation of graphical and algebraic interpretations of Figure 14A and B.

Summary and discussion of the increasing blanket thickness and complete incremental leaching models

The observation that the average enriched zone metal grade increases as a linear function of the total leached depth has been incorporated in two contrasting models for the dynamic evolution of supergene geochemical systems: the increasing blanket thickness and the complete incremental leaching models introduced above. Both models are based on the expression in eq. (4) for mass balance in redistributive geochemical profiles, taking different combinations of variables as constants as a function of the progress variable, z_R (depth of redox boundary). Both models refer to a transient ground-water flow regime with a net descending water table and redox boundary.

The increasing blanket thickness model (Fig. 13) refers to a relatively sudden hydrologic disturbance, where the rate of water table descent is rapid relative

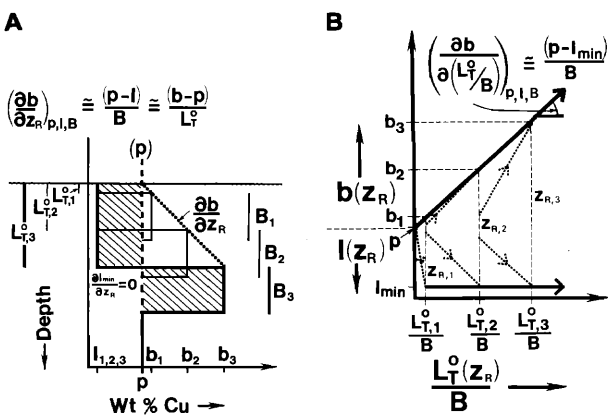

FIG. 14. Complete incremental leaching model for dynamic evolution of supergene enrichment system. A. Schematic plot of copper grade vs. depth, showing descent of redox front at constant enriched zone thickness, B_n. Average leached zone metal grade reaches minimum value, $l_{min}(=l_1 = l_2 = l_3)$, after each incremental descent of the redox front. Shaded areas ($n = 3$) are equal in area because of mass balance constraints, as in Figure 13A (see Appendix II). B. Schematic plot of $b(z_R)$ and $l(z_R)$ vs. $\frac{L^0_T(z_R)}{B}$, showing increase of $b(z_R)$ with increasing $\frac{L^0_T(z_R)}{B}$ at a constant slope equal to $\frac{(p - l_{min})}{B}$, neglecting density terms.

to the rate of sulfide oxidation in the leached zone. In contrast, the complete incremental leaching model (Fig. 14) refers to a more gradually changing water level, with sufficient time between incremental drops of the water table to allow for complete leaching of sulfides newly exposed to oxidation. The increasing blanket thickness model provides a description of the growth of the enrichment zone in both grade and thickness as the leached zone grade is gradually depleted, whereas the complete incremental leaching model describes the depletion of leached zone grade to its minimum value (l_{min}) for each incremental drop in water table elevation with a constant blanket thickness.

The increasing blanket thickness model is characterized by a continuous increase of the enriched blanket thickness (B) in proportion to the total leached column height (L_T^0) with a continuously decreasing average leached capping grade (1). This model leads to eventual attainment of a maximum blanket grade (b_{max}) when the minimum average leached capping grade (l_{min}) is reached. These grades are likely to vary among different rock types and alteration assemblages in a single deposit, depending largely on the Me/S ratio in sulfides, the total sulfide content, and the reactivity of wall rock. In contrast, no maximum grade is implied for the enriched zone in the complete incremental leaching model, except by cessation of conditions favorable to oxidative weathering, including climatic, hydrologic, and geomorphic regimes.

In natural systems, it is conceivable that both models may apply at different times during the evolution of a single supergene system and over different time scales. Factors such as climate, bacterial activity, topography, and tectonic history significantly influence the relative rates of sulfide oxidation, erosion, and ground-water table descent. We infer that faster erosion rates associated with more humid climates would favor the increasing blanket thickness model. Conversely, more arid climates would favor the complete incremental leaching model, providing that sufficient infiltrating water is available to flush the oxidation products from the oxidized zone to the reduced zone below the water table.

Supergene evolution at La Escondida, as recorded in the limonite assemblages in the leached capping zone, is consistent with the complete incremental leaching model for the overall supergene evolution of the deposit, given the essentially complete copper leaching evident in vertical profiles such as those in Figures 11 and 12. However, the increasing blanket thickness model may have been operative for certain portions of the supergene history.

The above models are considered valid only in the absence of perturbations, such as fault displacements or major climatic changes, which have significant impacts on the hydrologic setting. For example, such an event may have been partly responsible for raising the water table at La Escondida above the present top of sulfides throughout most of the district, acting along with regional climatic desiccation to preserve the system from further oxidation since the middle Miocene (Alpers et al., 1984; Brimhall et al., 1985; Alpers and Brimhall, 1988).

Estimation of lateral copper flux

The downhole mapping data can be used to carry out an approximate check on whether or not a given vertical profile is balanced in terms of lateral copper flux. This check is independent of the mass balance calculations described by Brimhall et al. (1985), which are based on an inventory of hypogene and supergene copper in a given profile. The rate of increase of enrichment blanket copper grade, b_α, with depth can be quantified as the slope $\frac{\partial b_\alpha}{\partial z}$ for each vertical profile by linear regression of the downhole mapping data in each profile. To assess whether or not the rate of increase of former blanket grades with depth is consistent with closed-system mass balance constraints and therefore could have taken place without significant lateral copper fluxes, the slope $\frac{\partial b_\alpha}{\partial z}$ is compared with the parameter $\left(\frac{\partial b}{\partial z_R}\right)_{CIL}$, which was defined in eq. (7) as $\left(\frac{\partial b}{\partial z_R}\right)_{CIL} \equiv \frac{(p\rho_p - l\rho_l)}{B\rho_b}$. The derivatives $\frac{\partial b_\alpha}{\partial z}$ and $\left(\frac{\partial b}{\partial z_R}\right)_{CIL}$ can be compared because it is assumed that each value of b_α represents a reconstructed blanket grade for a different location of the redox front. Evaluating $\left(\frac{\partial b}{\partial z_R}\right)_{CIL}$ for the profile in Figure 11 yields:

$$\left(\frac{\partial b}{\partial z_R}\right)_{CIL} = \frac{0.89\%\ \text{Cu}\ (2.57\ \text{g/cm}^3) - 0.12\%\ \text{Cu}\ (2.50\ \text{g/cm}^3)}{152\ \text{m}\ (2.55\ \text{g/cm}^3)}$$

$= 0.00513\%$ Cu/m, which is in remarkable agreement with the slope calculated by regression from the limonite mapping data: $\frac{\partial b_\alpha}{\partial z} = 0.00509$ percent Cu/m.

The drill holes shown in Figures 11 and 12 are located in a part of the Escondida district with little indicated lateral copper flux, based on bulk mass bal-

ance calculations (Brimhall et al., 1985) which assumed leaching from an original top of copper sulfides at 3,300 m above sea level, near to the present topographic surface in this portion of the deposit. This lack of overall lateral flux is consistent with the approximate equality of $\frac{\partial b_\alpha}{\partial z}$ and $\left(\frac{\partial b}{\partial z_R}\right)_{CIL}$ for this profile. For the other 12 vertical leached capping profiles mapped in detail, those with little or no indicated lateral flux also show values of $\frac{\partial b_\alpha}{\partial z}$ which agree closely with $\left(\frac{\partial b}{\partial z_R}\right)_{CIL}$ evaluated using copper grade and bulk density data from the individual profiles. In contrast, the profiles with evidence of positive lateral flux (sink regions) based on mass balance calculations as described by Brimhall et al. (1985), exhibit values of the slope $\frac{\partial b_\alpha}{\partial z}$ greater than $\left(\frac{\partial b}{\partial z_R}\right)_{CIL}$, consistent with positive lateral flux into those profiles. Profiles with net negative values of lateral flux (source regions) show values of $\frac{\partial b_\alpha}{\partial z}$ less that $\left(\frac{\partial b}{\partial z_R}\right)_{CIL}$.

The lower portion of the leached capping zone in the b_α vs. depth profiles in Figures 11 and 12 show a significantly higher slope, $\frac{\partial b_\alpha}{\partial z} \approx 0.010$ percent Cu/m, over a vertical interval of about 100 m in both profiles. Given that these vertical holes are only 200 m apart (Fig. 8), this interval of increased slope can be correlated with some confidence between these profiles. The increased slope could indicate lateral flux of copper into both profiles during late stages of supergene evolution, or alternatively, could represent a fundamental change of the physical and chemical properties of the rock type and/or wall-rock alteration with depth in this area. Note that the hypogene alteration in these profiles shows significant vertical variations (Figs. 11 and 12). Reductions in permeability due to precipitation of supergene minerals would certainly have affected the hydrology locally and could have led to the formation of a relatively thinner enrichment blanket of higher average grade toward the end stages of the leaching and enrichment process. Carried to the extreme, the precipitation of secondary phases such as supergene kaolinite, alunite, and chalcocite could serve to reduce permeability to the extent that downward infiltration would be significantly reduced and lateral ground-water fluxes could then result. This mechanism may account for the lateral migration of copper-rich solutions from the oxidized zone of some supergene systems, manifested as exotic chysocolla-atacamite mineralization in river gravels as at the Exotica mine, near Chuquicamata, Chile (Newberg, 1967; Mortimer et al., 1977).

Estimation of total leached column height and paleotopography

Vertical profiles of b_α may also be used to estimate the total thickness of the zone of oxidation and copper leaching, including eroded material. This is best accomplished by using b_α profiles in conjunction with mass balance calculations. If we consider that the blanket grade starts out equal to the protore grade and then increases according to eq. (4), then the elevation where the blanket grade was originally equal to the protore grade should define the point in space where enrichment began. In the following discussion, we assume that the protore grade is constant for each individual vertical profile. Thus, the elevation where mapped b_α equals the protore grade defines an elevation which we will call $SL_{T,\alpha}$, corresponding in principle to the elevation of the first copper enrichment for that vertical profile. The corresponding total leached column height $L_{T,\alpha}$ is defined by $L_{T,\alpha} = SL_{T,\alpha} - ETB$, where ETB is the elevation of the present top of the sulfide enrichment blanket (see Fig. 12).

In the case where $SL_{T,\alpha}$ is above the present surface (i.e., $b_\alpha > p$ at the surface), erosion of formerly enriched and subsequently leached material is indicated. It is of interest to compare values of $SL_{T,\alpha}$ with the analogous but independently calculated parameter SL_T^0, defined as the sum of elevation ETB and distance L_T^0, which can be calculated for each drill hole from the mass balance expression in eq. (3). For the profile in Figure 11, the $SL_{T,\alpha}$ and SL_T^0 parameters agree within 20 m, providing confirmation of the balanced nature of this profile with respect to negligible net lateral copper flux.

Also note in Figure 11 that the elevations $SL_{T,\alpha}$ and SL_T^0 are near a change in lithology in this profile. The upper 80 m of drill hole 219 is made up of pyritic rhyolitic porphyry (Alpers, 1986). Beneath the rhyolitic porphyry, the andesite was much richer in hypogene copper-iron sulfides. It is concluded that only a weak copper sulfide enrichment blanket was present as the water table descended through the rhyolitic porphyry and that significant copper enrichment began only when the water table reached the andesite.

To estimate the magnitude of lateral metal fluxes in sulfide weathering profiles, it is necessary to assume values for the total leached column height (Brimhall et al., 1985). In the absence of geologic or geomorphic constraints such as a regional erosional surface, one may be forced to make a variety of relatively unconstrained assumptions which can be difficult to test. The mapping methods described here provide a complementary approach to the mass balance methods because they provide such an independent geologic constraint. The parameter $SL_{T,\alpha}$, an estimate of the elevation of the top of copper sulfides at the beginning stages of supergene metal transport deduced by

quantitative limonite mapping, can be used in conjunction with mass balance calculations to determine the magnitude of lateral fluxes in complex natural systems.

Concluding Remarks

"It is to be expected that further applications of the outcrop technique will define the conditions of cumulative enrichment and yield improved means for its recognition." Augustus Locke (1926, p. 158).

Mapping of limonite mineralogy, texture, and abundance in vertical diamond drill cores from La Escondida provides the first quantitative evidence to support the concept of cumulative enrichment in supergene metal transport systems, as first proposed by Locke (1926). Systematic changes have been observed in the reconstructed enriched copper grade (b_α) and the former pyrite chalcocite ratio ($(py/cc)_\alpha$) down vertical profiles. This downhole mapping explains apparent discrepancies between the reconstructed preoxidation copper grade and sulfide mineralogy of surface exposures and the actual copper grade and mineralogy in the present underlying zone of sulfide enrichment. The limonite minerals preserved in the leached capping zone at La Escondida record the progressive evolution of copper grade and sulfide mineralogy of the enriched chalcocite zone as it descended through the rock column in response to a gradually descending water table and redox front.

In addition to the effect of cumulative sulfide enrichment on copper grade, progressively more complete replacement of pyrite by chalcocite occurs with increasing maturity of the enrichment process (Bateman, 1950; Blain and Andrew, 1977; Titley, 1982). This leads to a reduction of the Me/S ratio in the chalcocite zone as it descends through the rock column. Eventually, this mineralogic evolution will lead to the formation of copper oxide and sulfate minerals in the leached capping zone, as the py/cc ratio falls below 1:2.8 (Table 1). This effect, combined with a low hypogene pyrite content in the central portion of the district at La Escondida, accounts for the locally significant copper sulfate mineralization in the leached capping overlying the thickest and highest grade portion of the enrichment blanket, a zone with relatively nonreactive alteration otherwise favorable to efficient copper leaching.

An estimate of the total leached column height (including any eroded material) can be made if protore grades are known at depth by reconstructing enrichment blanket grades in vertical profiles through leached capping rocks. For vertical profiles with negligible net lateral copper flux during weathering, the estimate based on reconstructive limonite mapping is found to agree closely with independent estimates based on copper mass balance (Brimhall et al., 1985). For drill holes with significant lateral fluxes, quantitative limonite mapping yields an estimate of total leached column height which can be used to calculate the magnitude of lateral flux using the mass balance equations. Thus, the quantitative evaluation of former enriched zone grades in vertical profiles through leached cappings provides a method complementary to the mass balance approach. The detailed mapping of limonites is therefore an essential tool to be used in reconstruction of the paleohydrology, geomorphology, and geochemical evolution of fossil supergene systems.

The data and interpretations gathered from this type of analysis provide a sound basis on which to base numerical modeling efforts attempting to simulate the coupled chemical and physical response of sulfide-bearing rock systems to steady-state and transient ground-water flow during oxidative weathering (e.g., Bladh, 1982; Kwong et al., 1982; Cunningham, 1984; Lichtner, 1985; Narasimhan et al., 1985; Lichtner et al., 1987; Ague, 1987; Liu, 1988). Such modeling efforts are of increasing importance to understanding processes of supergene ore deposition and chemical weathering, as well as to solving environmental problems such as ground-water contamination by hazardous wastes and acid mine drainage (e.g., Chapman et al., 1982, 1983). Theoretical numerical modeling efforts would undoubtedly benefit from comparison with quantitative geologic and mineralogic descriptions of the spatial and chemical evolution of weathering systems over geologic time scales.

Acknowledgments

The authors would like to thank Utah International, Inc., Getty Minerals, Inc., and their subsidiary, Minera Utah de Chile, Inc. for financial and logistical support, access to data at La Escondida, and permission to publish these results. Jim Bratt of BHP-Utah International Minerals deserves special recognition for initiating and sustaining the authors' work at La Escondida. Financial support from the National Science Foundation through grant EAR 84-16790 to Brimhall is also gratefully acknowledged. J.K. Böhlke, Bill Chavez, J. Harold Courtright, Aric Cunningham, Bill Dietrich, Harvey Doner, J. David Lowell, Bill Murphy, T.N. Narasimhan, D. Kirk Nordstrom, and Roger Stoffregen have contributed to this study with helpful comments and suggestions. Critical comments by two anonymous *Economic Geology* reviewers helped improve the manuscript considerably.

October 1, 1986; August 25, 1988

REFERENCES

Aagaard, P., and Helgeson, H. C., 1982, Thermodynamic and kinetic constraints on reaction rates among minerals and aqueous solutions. I. Theoretical considerations: Am. Jour. Sci., v. 282, p. 237–285.

Ague, J. J., 1987, Geochemical modelling of fluid flow and chem-

ical reaction during supergene enrichment of porphyry copper deposits: Unpub. Ph.D. thesis, Berkeley, Univ. California, 62 p.

Alcayaga, C. S., 1984, Caracteres geologicos y metalogenicos del sector NW del yacimiento La Escondida, II Region de Antofagasta, Chile: Unpub. titular thesis, Antofagasta, Chile, Univ. del Norte, 113 p.

Alpers, C. N., 1986, Geochemical and geomorphological evolution of supergene copper sulfide ore formation and preservation at La Escondida, Antofagasta, Chile: Unpub. Ph.D. thesis, Berkeley, Univ. California, 184 p.

Alpers, C. N., and Brimhall, G. H, 1988, Middle Miocene climatic change in the Atacama Desert, northern Chile: Evidence from supergene mineralization at La Escondida: Geol. Soc. America Bull., v. 100, p. 1640–1656.

Alpers, C. N., Brimhall, G. H, Cunningham, A. B., and Burns, P. J., 1984, Mass balance and timing of supergene enrichment at La Escondida, Antofagasta Province, Chile [abs.]: Geol. Soc. America Abstracts with Programs, v. 16, p. 428.

Alpers, C. N., Nordstrom, D. K., and Ball, J. W., 1988, An evaluation of the solubility product constant of jarosite from oxidized mine waters aged 12 year [abs.]: Terra Cognita, v. 8, p. 178.

—— 1989, Solubility of jarosite solid solutions precipitated from acid mine waters, Iron Mountain, California, U.S.A.: Sci. Géol., (in press).

Ambrus, J., 1979, Emplazamiento y mineralización de los porfidos cupriferos de Chile: Unpub. Ph.D. thesis, Salamanca, Spain, Univ. Salamanca, 314 p.

—— 1980, Geologia de los porfidos cupriferos de Chile, *in* Minería de Cobres Porfidicos, v. 3: Santiago, Inst. Ing. Minas Chile, p. 9–51.

Anderson, J. A., 1982, Characteristics of leached capping and techniques of appraisal, *in* Titley, S. R., ed., Advances in geology of the porphyry copper deposits, southwestern North America: Tucson, Univ. Arizona Press, p. 275–295.

Andrew, R. L., 1980, Supergene alteration and gossan textures of base-metal ores in southern Africa: Minerals Sci. Eng., v. 12, p. 193–215.

Ball, J. W., Nordstrom, D. K., and Jenne, E. A., 1980, Additional and revised thermochemical data and computer code for WATEQ2—a computerized chemical model for trace and major element speciation and mineral equilibria of natural waters: U. S. Geol. Survey Water Resource Inv. 78–116, 109 p.

Ball, J. W., Nordstrom, D. K., and Zachmann, D. W., 1987, WATEQ4F—a personal computer FORTRAN translation of the geochemical model WATEQ2 with revised data base: U. S. Geol. Survey Open-File Rept. 87–50, 108 p.

Bateman, A. M., 1950, Economic mineral deposits: New York, John Wiley, p. 245–287.

Beane, R. E., and Titley, S. R., 1981, Porphyry copper deposits. Part II. Hydrothermal alteration and mineralization: ECON. GEOL. 75TH ANNIV. VOL., p. 235–269.

Berner, R. A., 1969, Goethite stability and the origin of red beds: Geochim. et Cosmochim. Acta, v. 33, p. 267–273.

—— 1971, Principles of chemical sedimentology: New York, McGraw-Hill, 240 p.

Bird, M. I., 1988, An isotopic study of the Australian regolith: Unpub. Ph.D. thesis, Canberra, Australian Natl. Univ., 241 p.

Bladh, K. W., 1978, The weathering of sulfide-bearing rocks associated with porphyry copper deposits: Unpub. Ph.D. thesis, Tuscon, Univ. Arizona, 98 p.

—— 1982, The formation of goethite, jarosite, and alunite during the weathering of sulfide-bearing felsic rocks: ECON. GEOL., v. 77, p. 176–184.

Blain, C. F., and Andrew, R. L., 1977, Sulfide weathering and the evaluation of gossans in mineral exploration: Minerals Sci. Eng., v. 9, p. 119–149.

Blanchard, R., 1968, Interpretation of leached outcrops: Nevada Bur. Mines Bull., v. 66, 196 p.

Bohmhammel, K., Naumann, R., and Paulik, F., 1987, Thermoanalytical and calorimetric investigations on the formation and decomposition of some alunites: Thermochim. Acta, v. 121, p. 109–119.

Brady, K. S., Bigham, J. M., Jaynes, W. F., and Logan, T. J., 1986, Influence of sulfate on Fe-oxide formation: Comparisons with a stream receiving acid mine drainage: Clays and Clay Minerals, v. 34, p. 266–274.

Brimhall, G. H, Jr., 1979, Lithologic determination of mass transfer mechanisms of multiple-stage porphyry copper mineralization at Butte, Montana: Vein formation by hypogene leaching and enrichment of potassium-silicate protore: ECON. GEOL., v. 74, p. 556–589.

Brimhall, G. H, Jr., and Dietrich, W. E., 1987, Constitutive relations between chemical composition, volume, density, porosity, and strain in metasomatic hydrothermal systems: Results on weathering and pedogenesis: Geochim. et Cosmochim. Acta, v. 51, p. 567–587.

Brimhall, G. H, Jr., and Ghiorso, M. S., 1983, Origin and ore-forming consequences of the advanced argillic alteration process in hypogene environments by magmatic gas contamination of meteoric fluids: ECON. GEOL., v. 78, p. 73–90.

Brimhall, G. H, and Rivers, M. H., 1985, Semi-automatic optical scanning apparatus using line integration: U. S. patent No. 4,503,555.

Brimhall, G. H, Jr., Alpers, C. N., and Cunningham, A. B., 1985, Analysis of supergene ore-forming processes and ground-water solute transport using mass balance principles: ECON. GEOL., v. 80, p. 1227–1256.

Briskey, J. A., Jr., and Bellamy, J. R., 1976, Bethlehem Copper's Jersey, East Jersey, Heustis, and Iona deposits: Canadian Inst. Mining Metallurgy Spec. Vol. 15, p. 105–119.

Brophy, G. P., and Sheridan, M. E., 1965, Sulfate studies IV. The jarosite-natrojarosite-hydronium jarosite solid solution series: Am. Mineralogist, v. 50, p. 1595–1607.

Brown, J. M., 1971, Jarosite-goethite stabilities at 25°C, 1 atm.: Mineralium Deposita, v. 6, p. 245–252.

Cailteux, J., 1974, Les sulfures du gisement cuprifère stratiforme de Musoshi, Shaba, Zaire, *in* Bartholomé, P., ed., Gisements stratiformes et provinces cuprifères: Liège, Soc. Geol. Belgique, p. 267–276.

Chapman, B. M., James, R. O., Jung, R. F., and Washington, H. G., 1982, Modelling the transport of reacting chemical contaminants in natural waters: Australian Jour. Marine Freshwater Research, v. 33, p. 617–628.

Chapman, B. M., Jones, D. R., and Jung, R. F., 1983, Processes controlling metal ion attenuation in acid mine drainage systems: Geochim. et Cosmochim. Acta, v. 47, p. 1957–1973.

Chukhrov, F., Zvijagin, B. B., Gorshkov, A. I., Erilova, L. P., and Balashova, V. V., 1973, Ferrihydrite: Akad. Nauk SSSR Izv., Ser. Geol., v. 4, p. 23–33.

Clark, A. H., 1972, A natural occurrence of hexagonal $Cu_{1.83}S$, Rancagua, Chile: Nature, v. 238, no. 86, p. 123–124.

Clark, A. H., and Sillitoe, R. H., 1971, Supergene anilite from Mina Estrella (Salado), Atacama, Chile: Neues Jahrb. Mineralogie Monatsh., 1971, p. 515–523.

Cummings, R. B., 1982, Geology of the Sacaton porphyry copper deposit, *in* Titley, S. R., ed., Advances in geology of the porphyry copper deposits, southwestern North America: Tucson, Univ. Arizona Press, p. 507–521.

Cunningham, A. B., 1984, Geologically-constrained hydrologic and geochemical modeling of supergene weathering processes using physical rock parameters, geochemical profiles and modal data: Unpub. M.S. thesis, Berkeley, Univ. California, 122 p.

Davison, W., and Seed, G., 1983, The kinetics of the oxidation of ferrous iron in synthetic and natural waters: Geochim. et Cosmochim. Acta, v. 47, p. 67–79.

Dutrizac, J. E., 1982, Jarosite-type compounds and their application in the metallurgical industry, *in* Osseo-Asare, K., and Miller, J. D., eds., Hydrometallurgy—research, development, and practice: New York, Am. Inst. Mining Metall. Petroleum Engineers, p. 531–551.

—— 1983, Factors affecting alkali jarosite precipitation: Inst. Mining Metallurgy Trans., v. 14, sec. B, p. 531–539.
Dutrizac, J. E., and Kaiman, S., 1976, Synthesis and properties of jarosite-type compounds: Canadian Mineralogist, v. 14, p. 151–158.
Dutrizac, J. E., and MacDonald, R. J. C., 1974, Ferric iron as a leaching medium: Minerals Sci. Eng., v. 6, p. 59–100.
England, P. C., and Thompson, A. B., 1984, Pressure-temperature-time paths of regional metamorphism. I. Heat transfer during the evolution of regions of thickened continental crust: Jour. Petrology, v. 25, p. 894–928.
Eggleton, R. A., and Fitzpatrick, R. W., 1988, New data and a revised structural model for ferrihydrite: Clays and Clay Minerals, v. 36, p. 111–124.
Feitknecht, W., and Michaelis, W., 1962, Über die hydrolyse von eisen(III)-perchlorat-lösungen: Helvetica Chim. Acta, v. 45, p. 212–224.
Field, C. W., and Gustafson, L. B., 1976, Sulfur isotopes in the porphyry copper deposit at El Salvador, Chile: ECON. GEOL., v. 71, p. 1533–1548.
Fischer, W. R., and Schwertmann, U., 1975, The formation of hematite from amorphous iron (III) hydroxide: Clays and Clay Minerals, v. 23, p. 33–37.
Freeze, R. A., and Cherry, J. A., 1979, Groundwater: Englewood Cliffs, New Jersey, Prentice-Hall, 604 p.
Gablina, I. F., 1984, [Sulfides of the chalcocite series from localities of cuperiferous sandstones]: Zapiski Vsesoiuznogo Mineralogicheskogo Obshchestva, v. 113, no. 4, p. 430–443 (in Russian).
Garrels, R. M., 1954, Mineral species as a function of pH and oxidation reduction potentials with special reference to the zone of oxidation and secondary enrichment of sulfide ore deposits: Geochim. et Cosmochim. Acta, v. 5, p. 153–168.
Garrels, R. M., and Christ, C. L., 1965, Solutions, minerals, and equilibria: San Francisco, Freeman, Cooper, Co., 450 p.
Gaskin, A. R. J., 1975, Investigation of the residual iron ores of Tonkolili, Sierra Leone: Inst. Mining Metallurgy Trans., v. 84, sec. B, p. B98–B119.
Goble, R. J., 1981, The leaching of copper from anilite and the production of a metastable copper sulfide structure: Canadian Mineralogist, v. 19, p. 583–591.
Goldhaber, M. B., 1983, Experimental study of metastable sulfur oxyanion formation during pyrite oxidation at pH 6-9 and 30°C: Am. Jour. Sci., v. 283, p. 193–217.
Gustafson, L. B., and Hunt, J. P., 1975, The porphyry copper deposit at El Salvador Chile: ECON. GEOL., v. 70, p. 857–912.
Härtig, C., Brand, P., and Böhmhammel, K., 1984, Fe-Al isomorphie und strukturwasser in kristallen von jarosit-alunit-typ [Fe-Al isomorphism and structural water in crystals of the jarosite-alunite group]: Anorg. Allg. Chemie Zeitschr., v. 508, p. 159–164.
Helgeson, H. C., Kirkham, D. H., and Flowers, G. C., 1981, Theoretical prediction of the thermodynamic behavior of aqueous electrolytes at high pressures and temperatures. IV. Calculation of activity coefficients, osmotic coefficients, and apparent molal and standard and relative partial molal properties to 600°C and 5 kb: Am. Jour. Sci., v. 281, p. 1249–1516.
James, A. H., 1971, Hypothetical diagrams of several porphyry copper deposits: ECON. GEOL., v. 66, p. 43–47.
Kamilli, R. J., and Ohmoto, H., 1977, Paragenesis, zoning, fluid inclusions, and isotopic studies of the Finlandia vein, Colqui district, central Peru: ECON. GEOL., v. 72, p. 950–982.
Kämpf, N., and Schwertmann, U., 1982, Goethite and hematite in a climo-sequence in southern Brazil and their application in classification of kaolinitic soils: Geoderma, v. 29, p. 27–39.
Kashkay, C. M., Borovskaya, Y. B., and Babazade, M. A., 1975, Determination of $\Delta G^0_{f,298}$ of synthetic jarosite and its sulphate analogs: Geochemistry Internat., v. 12, p. 115–121. [translated from Geokhimiya, 1975, p. 778–784.]
Kelly, W. C., and Turneaure, F. S., 1970, Mineralogy, paragenesis, and geothermometry of the tin and tungsten deposits of the eastern Andes, Bolivia: ECON. GEOL., v. 65, p. 609–680.
King, J. R., 1982, Geology of the San Xavier North porphyry copper deposit, *in* Titley, S. R., ed., Advances in geology of the porphyry copper deposits, southwestern North America: Tucson, Univ. Arizona Press, p. 475–485.
Knight, R. J., and Sylva, R. N., 1974, Precipitation in hydrolysed iron (III) solutions: Jour. Inorg. Nucl. Chemistry, v. 36, p. 591–597.
Kubisz, J., 1964, [Minerals of the alunite-jarosite group]: Akad. Nauk Polska Prace Geol., v. 22, p. 1–93 (in Polish).
—— 1970, Studies on synthetic alkali-hydronium jarosites. I. Synthesis of jarosite and natrojarosite: Mineralogia Polonica, v. 1., p. 47–57.
Kwong, Y. T. J., Brown, T. H., and Greenwood, H. J., 1982, A thermodynamic approach to the understanding of the supergene alteration at the Afton copper mine, south-central British Columbia: Canadian Jour. Earth Sci., v. 19, p. 2378–2386.
Langmuir, D., 1971, Particle size effect on the reaction goethite = hematite + water: Am. Jour. Sci., v. 271, p. 147–156.
—— 1972, Correction—particle size effect on the reaction goethite = hematite + water: Am. Jour. Sci., v. 272, p. 972.
Langmuir, D., and Whittemore, D. O., 1971, Nonequilibrium systems in natural water chemistry: Advances Chemistry Ser. no. 106, p. 209–234.
Langton, J. M., 1972, Ore genesis in the Morenci-Metcalf district: Am. Inst. Mining Metall. Petroleum Engineers Preprint 72-I-47, 38 p.
Lichtner, P. C., 1985, Continuum model for simultaneous chemical reaction and mass transport in hydrothermal systems: Geochim. et Cosmochim. Acta, v. 49, p. 779–800.
Lichtner, P. C., Helgeson, H. C., and Murphy, W. M., 1987, Lagrangian and Eulerian representations of metasomatic alteration of minerals, *in* Helgeson, H. C., ed., Chemical transport in metasomatic processes: Boston, D. Reidel, p. 519–545.
Liu, C.-W., 1988, Multiple-species chemical transport involving oxidation/reduction reactions in geological media: Unpub. Ph.D. thesis, Berkeley, Univ. California, 257 p.
Locke, A., 1926, Leached outcrops as guides to copper ores: Baltimore, Williams Wilkins Co., 166 p.
Loghry, J. D., 1972, Characteristics of favorable cappings from several southwestern porphyry copper deposits: Unpub. M.S. thesis, Tucson, Univ. Arizona, 112 p.
Loucks, R. R., 1982, Zoning and ore genesis, Topia, Durango, Mexico: Unpub. Ph.D. thesis, Harvard Univ., 416 p.
Lowell, J. D., 1968, Geology of the Kalamazoo orebody, San Manuel district, Arizona: ECON. GEOL., v. 63, p. 645–654.
Lowell, J. D., and Guilbert, J. M., 1970, Lateral and vertical alteration-mineralization zoning in porphyry ore deposits: ECON. GEOL., v. 65, p. 373–408.
Marcantonio, P. J., 1976, Chalcocite dissolution in acidic ferric-sulfate solutions: Unpub. Ph.D. thesis, Salt Lake City, Univ. Utah, 138 p.
Maynard, J. B., 1983, Geochemistry of sedimentary ore deposits: New York, Springer-Verlag, 305 p.
McClave, M., 1973, Control and distribution of supergene enrichment in the Berkeley pit, Butte district, Montana, *in* Miller, R. N., ed., Guidebook for the Butte Field Meeting of Society Economic Geologists, Butte, Montana, Aug. 18–21, 1973: Butte, Montana, Anaconda Co., p. K1–K4.
Morimoto, N., and Gyobu, A., 1971, The composition and stability of digenite: Am. Mineralogist, v. 56, p. 1889–1909.
Mortimer, C., 1973, The Cenozoic history of the southern Atacama Desert, Chile: Geol. Soc. London Jour., v. 129, p. 505–526.
Mortimer, C., and Sarič-Rendic, N., 1975, Cenozoic studies in northern Chile: Geol. Rundsch., v. 64, p. 395–420.
Mortimer, C., Munchmeyer, C., and Urqueta, M., 1977, Emplacement of the Exótica ore body, Atacama Desert, Chile: Inst. Mining Metallurgy Trans., v. 86, sec. B, p. B121–B127.
Munsell Color Company, 1975, Munsell® soil color charts, 1975 Edition: Baltimore, Munsell Color Co., 4 p.
Murray, J. W., 1979, Iron oxides: Rev. Mineralogy, v. 6., p. 47–98.

Narasimhan, T. N., White, A., and Takeneda, T., 1985, Multiple species chemical transport with precipitation and dissolution: A case history, *in* Earth Science Division Annual Report, 1984: Berkeley, California, Lawrence Berkeley Laboratory, p. 140–143.

Naumov, G. B., Ryzhenko, B. N., and Khodakovsky, I. L., 1971, Handbook of thermodynamic data: Moscow, Atomizdat, 328 p. (Translated by G. J. Soleimani, U. S. Geol. Survey, 1974, NTIS PB-226 722).

Newberg, D. W., 1967, Geochemical implications of chrysocolla-bearing alluvial gravels: ECON. GEOL., v. 62, p. 932–956.

Nordstrom, D. K., 1977, Hydrogeochemistry and microbiological factors affecting the heavy metal chemistry of an acid mine drainage system: Unpub. Ph.D. thesis, Stanford Univ., 210 p.

—— 1982, Aqueous pyrite oxidation and the consequent formation of secondary iron minerals: Soil Sci. Soc. America Spec. Pub. 10, p. 37–46.

Nordstrom, D. K., and Munoz, J. L., 1986, Geochemical thermodynamics: Palo Alto, California, Blackwell Scientific, 477 p.

Nordstrom, D. K., Jenne, E. A., and Ball, J. W., 1979, Redox equilibria of iron in acid mine waters: American Chem. Soc. Symposium Ser., v. 93, p. 51–79.

Ohmoto, H., and Lasaga, A. L., 1982, Kinetics of reactions between aqueous sulfates and sulfides: Geochim. et Cosmochim. Acta, v. 46, p. 1727–1745.

Posnjak, E., and Merwin, H. E., 1922, The system Fe_2O_3-SO_3-H_2O: Am. Chem. Soc. Jour., v. 44, p. 1965–1994.

Potter, R. W. II, 1977, An electrochemical investigation of the system copper-sulfur: ECON. GEOL., v. 72, p. 1524–1542.

Richard, K., and Courtright, J. H., 1958, Geology of Toquepala, Peru: Mining Eng., Feb., 1958, p. 262–266.

Ripley, E. M., Lambert, M. W., and Berendsen, P., 1980, Mineralogy and paragenesis of red-bed copper mineralization in the Lower Permian of south central Kansas: ECON. GEOL., v. 75, p. 722–729.

Ripmeester, J. A., Ratcliffe, C. I., Dutrizac, J. E., and Jambor, J. L., 1986, Hydronium ion in the alunite-jarosite group: Canadian Mineralogist, v. 24, p. 435–447.

Robie, R. A., Hemingway, B. S., and Fisher, J. R., 1978, Thermodynamic properties of minerals and related substances at 298.15 K and 1 bar (10^5 Pascals) pressure and at higher temperatures: U. S. Geol. Survey Bull. 1452, 456 p. [reprinted in 1979 with corrections].

Rose, A. W., Jr., 1970, Zonal relationships of wallrock alteration and sulfide distribution at porphyry copper deposits: ECON. GEOL., v. 65, p. 920–936.

Roseboom, E. H., Jr., 1966, An investigation of the system Cu-S and some natural copper sulfides between 25° and 700°C: ECON. GEOL., v. 61, p. 641–672.

Russell, J. D., 1979, Infrared spectroscopy of ferrihydrite: Evidence for the presence of structural hydroxyl groups: Clay Minerals, v. 14, p. 109–113.

Sangameshwar, S. R., and Barnes, H. L., 1983, Supergene processes in zinc-lead-silver sulfide ores in carbonates: ECON. GEOL., v. 78, p. 1379–1397.

Sato, M., 1960, Oxidation of sulfide ore bodies: 1. Geochemical environments in terms of Eh and pH: ECON. GEOL., v. 55, p. 928–961.

Schellmann, W., 1959, Experimentelle untersuchungen über die sedimentäre bildung von goethit und hämatit: Chemie der Erde, v. 20, p. 104–135.

Schulze, D. G., 1984, The influence of aluminum on iron oxides. VIII. Unit-cell dimensions of Al-substituted goethites and estimation of Al from them: Clays and Clay Minerals, v. 32, p. 36–44.

Schwertmann, U., 1965, Zur goethit- und hämatitbildung aus amorphem eisen (III)-hydroxid: Bodenk Zeitschr. Pflanzenernährung. Düngung, Bodenkunde, v. 108, p. 37–45.

—— 1969, Die bildung von eisenoxidmineralen: Fortschr. Mineralogie, v. 46, p. 274–285.

—— 1985, The effect of pedogenic environments on iron oxide minerals: Adv. Soil Science, v. 1, p. 172–200.

Schwertmann, U., and Fischer, W., 1965, Zur bildung von α-FeOOH and α-Fe_2O_3 aus amorphem eisen(III)-hydroxid: Anorg. Allg. Chemie Zeitschr., v. 346, p. 137–142.

Schwertmann, U., and Murad, E., 1983, Effect of pH on the formation of goethite and hematite from ferrihydrite: Clays and Clay Minerals, v. 31, p. 277–284.

Sillitoe, R. H., 1981, Regional aspects of the Andean porphyry copper belt in Chile and Argentina: Inst. Mining Metallurgy Trans., v. 90, sec. B, p. B15–B36.

Sillitoe, R. H., and Clark, A. H., 1969, Copper and copper-iron sulfides as the initial products of supergene oxidation, Copiapó mining district, Chile: Am. Mineralogist, v. 54, p. 1684–1710.

Sillitoe, R. H., Jamarillo, L., and Castro, H., 1984, Geologic exploration of a molybdenum-rich porphyry copper deposit at Mocoa, Colombia: ECON. GEOL., v. 79, p. 106–123.

Sillitoe, R. H., Mortimer, C., and Clark, A. H., 1968, A chronology of landform evolution and supergene mineral alteration, southern Atacama Desert, Chile: Inst. Mining Metallurgy Trans. v. 77, sec. B, p. B166–B169.

Silman, J. F. B., 1958, The stabilities of some oxidized copper minerals in aqueous solutions at 25° C and 1 atmosphere total pressure: Unpub. Ph.D. thesis, Harvard Univ., 98 p.

Singer, P. C., and Stumm, W., 1970, Acid mine drainage: The rate determining step: Science, v. 167, p. 1121–1123.

Stoffregen, R. E., and Alpers, C. N., 1987, Woodhouseite and svanbergite in hydrothermal ore deposits: Products of apatite destruction during advanced argillic alteration: Canadian Mineralogist, v. 25, p. 201–211.

Tardy, Y., and Nahon, D., 1985, Geochemistry of laterites, stability of Al-goethite, Al-hematite, and Fe^{3+}-kaolinite in bauxites and ferricretes: An approach to the mechanism of concretion formation: Am. Jour. Sci., v. 285, p. 865–903.

Taylor, R. M., and Grayley, A. M., 1967, The influence of ionic environment on the nature of iron oxides in soils: Jour. Soil Sci., v. 18, p. 341–348.

Thornber, M. R., 1975, Supergene alteration of sulfides, II. A chemical study of the Kambalda nickel deposits: Chem. Geology, v. 15, p. 117–144.

—— 1985, Supergene alteration of sulfides, VII. Distribution of elements during the gossan-forming process: Chem. Geology, v. 53, p. 279–301.

Titley, S. R., 1982, The style and progress of mineralization and alteration in porphyry copper systems, American southwest, *in* Titley, S. R., ed., Advances in geology of the porphyry copper deposits, southwestern North America: Tucson, Univ. Arizona Press, p. 93–116.

Torrent, J., and Guzman, R., 1982, Crystallization of Fe(III)-oxides from ferrihydrite in salt solutions: Osmotic and specific ion effects: Clay Minerals, v. 17, p. 463–469.

Torrent, J., Schwertmann, U., and Schulze, D. G., 1980, Iron oxide mineralogy of some soils of two river terrace sequences in Spain: Geoderma, v. 23, p. 191–208.

Tosdal, R. M., 1978, The timing of the geomorphic and tectonic evolution of the southwesternmost Peruvian Andes: Unpub. M.Sc. thesis, Kingston, Ontario, Queen's Univ., 136 p.

Trolard, F., and Tardy, Y., 1987, The stabilities of gibbsite, boehmite, aluminous goethites, and aluminous hematites in bauxites, ferricretes, and laterites as a function of water activity, temperature, and particle size: Geochim. et Cosmochim. Acta, v. 51, p. 945–957.

Tunell, G., 1930, The oxidation of disseminated copper ores in altered porphyry: Unpub. Ph.D. thesis, Harvard Univ., 102 p.

van Breemen, N., 1973, Soil forming processes in acid sulfate soils, *in* Dost, H., ed., Acid sulfate soils: Wageningen, Netherlands, Internat. Inst. Land Reclamation Improvement, v. 1, p. 66–128.

Wagman, D. D., Evans, W. H., Parker, V. B., Schumm, R. H., Halow, I., Bailey, S. M., Churney, K. L., and Nuttall, R. L., 1982, The NBS tables of chemical thermodynamic properties: Selected values for inorganic and C_1 and C_2 organic substances in SI units: Jour. Phys. Chemistry Reference Data, v. 11 (supp. 2), p. 1–392.

Whittemore, D. O., 1973, The chemistry and mineralogy of ferric oxyhydroxides precipitated in sulfate solutions: Unpub. Ph.D. thesis, Pennsylvania State Univ., 159 p.

Wiersma, C. L., and Rimstidt, J. D., 1984, Rates of reaction of pyrite and marcasite with ferric iron at pH 2: Geochim. et Cosmochim. Acta, v. 48, p. 85–92.

Woods, T. L., and Garrels, R. M., 1986, Phase relations of some cupric hydroxy minerals: ECON. GEOL., v. 81, p. 1989–2007.

Yapp, C., 1983, Effects of AlOOH-FeOOH solid solution on goethite-hematite equilibrium: Clays and Clay Minerals, v. 31, p. 239–240.

APPENDIX I

Thermodynamic Data Used to Construct Figures 3 and 6

Formula	Mineral	State[1]	$\Delta G^\circ_{f,298}$ (kcal/mole)	log K_{sp}	Source[4]
Figure 3					
Minerals					
$KFe_3(SO_4)_2(OH)_6$	Jarosite	c	[−788.6][2]	−93.21	1, 2
α-FeO(OH)	Goethite	c	−117.2	[−41.7][3]	3
α-Fe_2O_3	Hematite	c	−177.44	[−41.6][3]	3
"$Fe(OH)_3$"	Ferrihydrite	pc	[−170.24][2]	−39.0	2
FeS_2	Pyrite	c	38.9		3
Aqueous species					
Fe^{+2}		aq	−22.05		3
Fe^{+3}		aq	−4.27		3
$FeSO_4^\circ$		aq	[−202.9][2]	2.25	4
$FeSO_4^+$		aq	[−187.4][2]	3.92	4
$FeHSO_4^+$		aq	[−204.0][2]	1.08	5
$FeHSO_4^{+2}$		aq	[−188.1][2]	2.48	5
H_2S		aq	−6.66		3
HS^-		aq	−2.88		3
HSO_4^-		aq	−180.48		3
SO_4^{-2}		aq	−177.78		3
K^+		aq	−67.557		3
OH^-		aq	−37.594		6
H_2O		l	−56.687		6
Figure 6					
Minerals					
CuS	Covellite	c	−12.887		7
$Cu_{1.75}S$	Anilite	c	−18.771		7
$Cu_{1.934}S$	Djurleite-I	c	−20.041		7
$Cu_{1.965}S$	Djurleite-II	c	−20.230		7
Cu_2S	Low chalcocite	c	−20.452		7
Cu	Native copper	c	0.0		Convention
Cu_2O	Cuprite	c	−34.894		8, 9
CuO	Tenorite	c	−30.091		10
$Cu_4(SO_4)(OH)_6$	Brochantite	c	−434.620		10, 11
S	Sulfur (rhombic)	c	0.0		Convention
Aqueous species					
Cu^+		aq	11.95		3
Cu^{+2}		aq	15.651		3
H_2S		aq	−6.66		3
HS^-		aq	−2.88		3
HSO_4^-		aq	−180.48		3
SO_4^{-2}		aq	−177.78		3
OH^-		aq	−37.594		6
H_2O		l	−56.687		6

Note: data from Naumov et al. (1971) were chosen for iron minerals and aqueous species, where available, for consistency with jarosite data from Kashkay et al. (1975); stability of goethite with respect to hematite (plus water) from data of Naumov et al. (1971) is consistent with results of Langmuir (1971, 1972)

[1] Abbreviations: aq = aqueous, c = crystalline, l = liquid, pc = poorly crystalline

[2] Gibbs free energy of formation values in brackets calculated from solubility product using data for aqueous species

[3] Solubility products (sp) in brackets calculated from Gibbs free energy values

[4] Sources of data: 1. Kashkay et al. (1975); 2. Chapman et al. (1983); 3. Naumov et al. (1971); 4. Ball et al. (1980); 5. Ball et al. (1987); 6. Helgeson et al. (1981); 7. Potter (1977); 8. Robie et al. (1978); 9. Wagman et al. (1982); 10. Woods and Garrels (1986); 11. Silman (1958)

APPENDIX II

Comparison of Algebraic and Graphical Interpretations for Increasing Blanket Thickness and Complete Incremental Leaching Models

Increasing blanket thickness model

The following discussion is designed to aid in the graphical interpretation of the increasing blanket thickness model, referring to Figure 13A and B. In Figure 13, the progress variable for enrichment, $z_R(n)$, is shown to change incrementally (n = 1, 2, 3, max). At any time after initiation of the leaching and enrichment process, for example n = 3, the change in average blanket grade with the progress variable, $\frac{\partial b}{\partial z_R}$ (represented by the slope of the heavy dotted line in Fig. 13A), is approximately equal to the difference between blanket grade and protore grade ($b_3 - p$) divided by the total distance leached ($L^0_{T,3}$):

$$\left(\frac{\partial b}{\partial z_R}\right)_{\frac{L^0_T}{B},p,\rho_l,\rho_b,\rho_p} \approx \frac{(b_3 - p)}{L^0_{T,3}}. \quad (A1)$$

Similarly, the change in average leached zone grade as a function of the progress variable, $\frac{\partial l}{\partial z_R}$ (represented by the slope of the lighter dotted line in Fig. 13A), is equal to the difference between leached zone grade and protore grade ($l_3 - p$) divided by the total distance leached:

$$\left(\frac{\partial l}{\partial z_R}\right)_{\frac{L^0_T}{B},p,\rho_l,\rho_b,\rho_p} \approx \frac{(l_3 - p)}{L^0_{T,3}}. \quad (A2)$$

We can use the mass balance expression in eq. (3) to relate eqs. (A1) and (A2) as a graphical check on the relationship in eq. (5). Neglecting the density terms, the mass balance expression evaluated at n = 3 yields:

$$B_3(b_3 - p) \approx L^0_{T,3}(p - l_3). \quad (A3)$$

Graphically, this approximate equality can be visualized by the equality of the shaded areas in Figure 13A. Rearranging eq. (A3) gives:

$$L^0_{T,3} \approx \frac{B_3(b_3 - p)}{(p - l_3)}. \quad (A4)$$

Substituting eq. (A4) into (A1) gives:

$$\left(\frac{\partial b}{\partial z_R}\right)_{\frac{L^0_T}{B},p,\rho_l,\rho_b,\rho_p} \approx \frac{(p - l_3)}{B_3}. \quad (A5)$$

From eq. (A2),

$$(p - l_3) \approx -L^0_{T,3}\left(\frac{\partial l}{\partial z_R}\right)_{\frac{L^0_T}{B},p,\rho_l,\rho_b,\rho_p}, \quad (A6)$$

and therefore,

$$\left(\frac{\partial b}{\partial z_R}\right)_{\frac{L^0_T}{B},p,\rho_l,\rho_b,\rho_p} \approx -\left(\frac{L^0_{T,3}}{B_3}\right)\left(\frac{\partial l}{\partial z_R}\right)_{\frac{L^0_T}{B},p,\rho_l,\rho_b,\rho_p}. \quad (A7)$$

Equation A7 is an expression equivalent to eq. (5) without the density terms, which were left out so that these simple derivatives can be assessed graphically in Figure 13A.

In Figure 13B, $b(z_R)$ and $l(z_R)$ are plotted schematically vs. ($p - l(z_R)$), again with density terms neglected for simplicity. This plot illustrates the linear interpretation of eq. (4), where the quotient $\frac{L^0_T}{B}$ is assumed to remain constant as a function of depth, corresponding to the slope of the heavy solid line in Figure 13B, as indicated. Graphically, it can be seen that:

$$\frac{L^0_{T,n}}{B_n} \approx \frac{(b_n - p)}{(p - l_n)}, \quad (A8)$$

which is an additional statement of mass balance equivalent to the expressions in eqs. (3), (A3), and (A4).

Complete incremental leaching model

Figure 14A and B show the geometric relationships of the complete incremental leaching model, again neglecting density terms for simplicity. For n = 3, the increase of blanket grade with depth is analogous to the expression in eq. (A1). Using the same mass balance arguments as above,

$$\left(\frac{\partial b}{\partial z_R}\right)_{B,p,l_{min},\rho_l,\rho_b,\rho_p} \approx \frac{(b_3 - p)}{L^0_{T,3}} \approx \frac{(p - l_3)}{B_3} \approx \frac{(p - l_{min})}{B_3}. \quad (A9)$$

Because l_{min} is constant as a function of z_R in this model, $\left(\frac{\partial l_{min}}{\partial z}\right)_{B,p,l_{min},\rho_l,\rho_b,\rho_p} = 0$, as shown in Figure 14A.

In Figure 14B, $b(z_R)$ is plotted vs. $\frac{L_T^0(z_R)}{B}$ to show an alternative linear interpretation of eq. (4), where term (4) is now constant and term (3) is the abscissa. The dotted lines in Figure 14B represent the paths of $b(z_R)$ and $l(z_R)$ between stages of water table descent. Each time the water table descends, the boundary between the leached zone and the enriched zone is redefined instantaneously before any leaching can occur, so that the copper formerly in the upper portion of the enrichment blanket zone is incorporated into the leached zone, which temporarily increases the average leached zone grade and temporarily decreases the average enriched zone grade. For small drops in the water table, these fluctuations from the overall slope would be small; however, for large changes in water table elevation, significant deviations from the line with slope $(p - l_{min})$ would result, as shown in Figure 14B. If the water table were to drop by a distance greater than the thickness of the enrichment blanket zone, these average grades l and b would return to their original values, equal to protore grade, p.